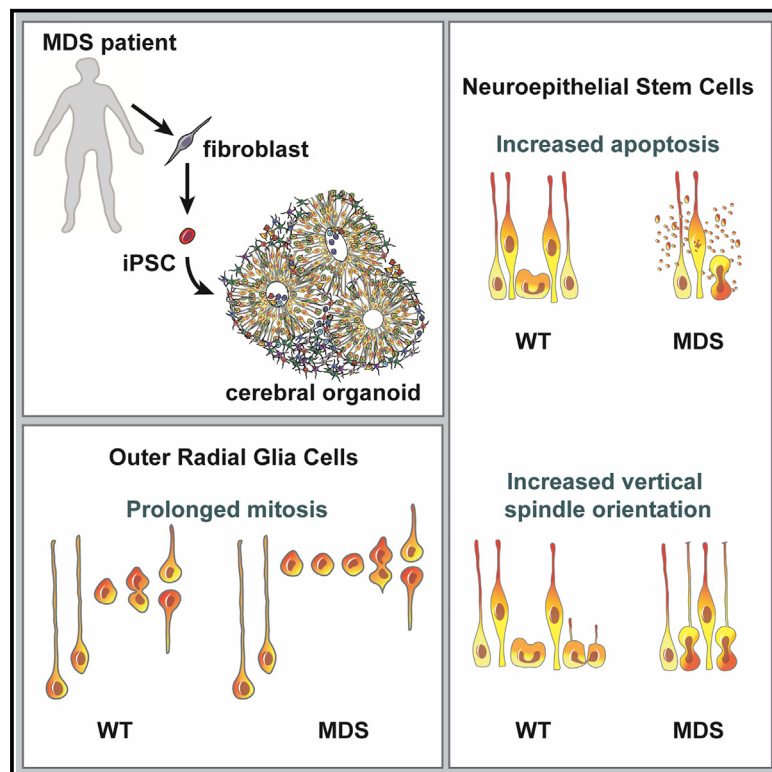


Human iPSC-Derived Cerebral Organoids Model Cellular Features of Lissencephaly and Reveal Prolonged Mitosis of Outer Radial Glia

Graphical Abstract



Authors

Marina Bershteyn,
Tomasz J. Nowakowski, Alex A. Pollen,
Elizabeth Di Lullo, Aishwarya Nene,
Anthony Wynshaw-Boris,
Arnold R. Kriegstein

Correspondence

mbershteyn@gmail.com (M.B.),
ajw168@case.edu (A.W.-B.),
kriegsteina@stemcell.ucsf.edu (A.R.K.)

In Brief

Bershteyn and colleagues show that cerebral organoid modeling of lissencephaly using iPSCs derived from Miller-Dieker syndrome patients can characterize cellular and neurodevelopmental disease phenotypes and identify a mitotic defect in outer radial glia, a cell type that is particularly important for human cortical development.

Highlights

- Cortical organoids from control and MDS patient-derived iPSCs model lissencephaly
- Neural stem cells in MDS organoids show increased apoptosis and horizontal divisions
- Deep-layer neurons are more abundant in MDS organoids than in controls
- Outer radial glia-like cells forming in MDS organoids show a mitotic delay

Human iPSC-Derived Cerebral Organoids Model Cellular Features of Lissencephaly and Reveal Prolonged Mitosis of Outer Radial Glia

Marina Bershteyn,^{1,2,6,*} Tomasz J. Nowakowski,^{1,3} Alex A. Pollen,^{1,3} Elizabeth Di Lullo,^{1,3} Aishwarya Nene,⁴ Anthony Wynshaw-Boris,^{2,5,*} and Arnold R. Kriegstein^{1,3,7,*}

¹Eli and Edythe Broad Center of Regeneration Medicine and Stem Cell Research, University of California, San Francisco, San Francisco, CA 94143, USA

²Institute for Human Genetics, University of California, San Francisco, San Francisco, CA 94143, USA

³Department of Neurology, University of California, San Francisco, San Francisco, CA 94143, USA

⁴California Institute of Technology, Pasadena, CA 91125, USA

⁵Department of Genetics and Genome Sciences, Case Western Reserve University, Cleveland, OH 44106, USA

⁶Present address: Neurona Therapeutics, South San Francisco, CA 94080, USA

⁷Lead Contact

*Correspondence: mbershteyn@gmail.com (M.B.), ajw168@case.edu (A.W.-B.), kriegsteina@stemcell.ucsf.edu (A.R.K.)

<http://dx.doi.org/10.1016/j.stem.2016.12.007>

SUMMARY

Classical lissencephaly is a genetic neurological disorder associated with mental retardation and intractable epilepsy, and Miller-Dieker syndrome (MDS) is the most severe form of the disease. In this study, to investigate the effects of MDS on human progenitor subtypes that control neuronal output and influence brain topology, we analyzed cerebral organoids derived from control and MDS-induced pluripotent stem cells (iPSCs) using time-lapse imaging, immunostaining, and single-cell RNA sequencing. We saw a cell migration defect that was rescued when we corrected the MDS causative chromosomal deletion and severe apoptosis of the founder neuroepithelial stem cells, accompanied by increased horizontal cell divisions. We also identified a mitotic defect in outer radial glia, a progenitor subtype that is largely absent from lissencephalic rodents but critical for human neocortical expansion. Our study, therefore, deepens our understanding of MDS cellular pathogenesis and highlights the broad utility of cerebral organoids for modeling human neurodevelopmental disorders.

INTRODUCTION

The human cerebral cortex develops from a pseudostratified layer of neuroepithelial stem cells (NESCs) into a functionally complex, six-layered structure with a folded (gyrencephalic) surface. The molecular underpinnings of brain size and topology are encoded by the genome and distinguish us from species with a small and smooth (lissencephalic) brain surface, such as mice. Although brain folding in the human does not begin until the end of the second trimester (after gestation week [GW] 23) (Chi et al., 1977; Martin et al., 1988; Hansen

et al., 1993; Armstrong et al., 1995), many of the key cellular events that influence this process, including expansion of the progenitor population and neuronal migration, occur starting around GW4 (Lui et al., 2011; Sidman and Rakic, 1973; Stiles and Jernigan 2010). Genetic and infectious diseases that disrupt these processes underlie a number of cortical malformations and cause mental retardation, mortality, and morbidity (Guerrini and Dobyns 2014; Hu et al., 2014). Despite the prevalence and societal burden of cortical malformations, our understanding of how disease-linked mutations disrupt brain development is still limited.

Miller-Dieker syndrome (MDS) is a severe cortical malformation characterized by nearly absent cortical folding (lissencephaly) often associated with reduced brain size (microcephaly), craniofacial dysmorphisms, mental retardation, and intractable epilepsy (Dobyns et al., 1983, 1991; Nagamani et al., 2009). MDS is caused by large heterozygous deletions of human band 17p13.3, harboring dozens of genes, including *PAFAH1B1* (LIS1 protein) and *YWHAE* (14-3-3 ϵ protein) (Dobyns et al., 1983; Reiner et al., 1993; Hattori et al., 1994; Chong et al., 1997; Cardoso et al., 2003). Smaller deletions or mutations in *PAFAH1B1* are the major cause of isolated lissencephaly sequence (ILS), which exhibits less severe degrees of lissencephaly (Ledbetter et al., 1992; Lo Nigro et al., 1997; Pilz et al., 1998; Barkovich et al., 1991; Cardoso et al., 2003). Insight into lissencephaly pathogenesis is largely derived from mouse models and limited analyses of postmortem human brains. Reduction in LIS1 levels in *Pafah1b1* mutant mice leads to defects in neuronal migration (Hirotsune et al., 1998; Smith et al., 2000), consistent with the disrupted cortical layering and neuron dispersion seen in the postmortem MDS brain (Sheen et al., 2006b; Saito et al., 2011). LIS1 is an atypical microtubule-associated protein that regulates microtubule dynamics and nuclear-centrosomal coupling during neuronal migration (Faulkner et al., 2000; Gambello et al., 2003; Shu et al., 2004; Tanaka et al., 2004; Youn et al., 2009). Collectively, these studies led to the prevailing model that lissencephaly is due to defective neuronal migration (Kato and Dobyns, 2003). However, the mouse brain is naturally lissencephalic,

suggesting that certain aspects of cortical development may not be adequately assessed in mice.

Recent work has uncovered critical cellular and molecular differences between cortical development in humans and mice, further underscoring the need to develop human model systems. In the developing human cortex, the outer subventricular zone (OSVZ) is greatly expanded (Smart et al., 2002; Lukaszewicz et al., 2005). OSVZ progenitors, which include transit-amplifying intermediate progenitor (IP) cells and outer or basal radial glia (oRG/bRG) (Hansen et al., 2010; Fietz et al., 2010; Betizeau et al., 2013), have been proposed to contribute to the majority of upper-layer neurogenesis (Smart et al., 2002; Lukaszewicz et al., 2005). Although IP cells are conserved between humans and mice, oRG cells are largely absent from the developing cortices of lissencephalic rodents (Shitamukai et al., 2011; Wang et al., 2011), which may explain why the phenotypes in *Pafah1b1^{+/−}* mice are substantially milder than in human patients with heterozygous *PAFAH1B1* mutations. Multiple lines of evidence suggest that the high abundance and proliferative capacity of oRG cells are critical for the vast developmental and evolutionary increase in cortical size (Stahl et al., 2013; Reillo et al., 2011).

To bridge the gap between mouse models and human disease, patient-derived induced pluripotent stem cells (iPSCs) (Takahashi et al., 2007; Yu et al., 2007; Park et al., 2008) represent a promising approach to study disease pathogenesis in a relevant genetic and cellular context. Human iPSCs provide a renewable source of neuronal progenitors and neurons, can be genetically and pharmacologically manipulated, and can recapitulate key cellular processes of *in vivo* brain development (Eiraku et al., 2008; Gaspard et al., 2008). Studies have shown that oRG-like cortical cells can be produced from human, but not mouse, iPSCs (Shi et al., 2012; Kadoshima et al., 2013; Lancaster et al., 2013; Qian et al., 2016), highlighting the advantage of the species-specific cellular model systems. However, the extent to which *in vitro*-derived oRG cells recapitulate the functional properties and molecular identity of primary oRG cells has not been determined. Here we implement a 3D cerebral organoid culture method (Kadoshima et al., 2013) to analyze the effect of MDS lissencephaly mutations on distinct biological processes and cell types corresponding to the first trimester of cortical development. Using a multifaceted approach integrating histology, live cell imaging, and single-cell transcriptomics, we uncover cell type-specific defects in lissencephaly spanning the stages of neuroepithelial cell expansion, neuronal migration, and the mitotic properties of oRG progenitors, providing deeper insight into human cortical development and lissencephaly.

RESULTS

Increased Apoptosis of NESCs in MDS Cortical Organoids

To study MDS pathogenesis, we generated iPSCs from three MDS individuals (Figures 1A–1C) using non-integrating episomal reprogramming vectors (Okita et al., 2011; Bershteyn et al., 2014). From each individual, we chose two independent iPSC clones with confirmed pluripotency, normal karyotype, and stable maintenance of the 17p13.3 deletion for subsequent studies (Bershteyn et al., 2014, and data not shown). To assess the effect

of MDS on NESCs, we implemented a published suspension culture method whereby equal numbers of dissociated iPSCs are quickly re-aggregated in serum-free cortical differentiation medium (Kadoshima et al., 2013). Initially and on day 3, there were no significant differences in the size of wild-type (WT) and MDS aggregates (Figures S1A and S1C). However, by 2.5 weeks of suspension culture (day 18 ± 1), the MDS organoids were significantly smaller (Figure 1D; Figures S1B–S1D). We observed that 25% of MDS organoids ($n = 3$ individuals, 2 iPSC clones each) were very small (less than 0.5 mm in circumference; Figure 1D) and invariably disintegrated before they could be analyzed. Of note, organoids derived from both of the MDS4 clones exhibited particularly poor growth in suspension and were therefore omitted from most of the subsequent assays.

The larger organoids were fixed and sectioned after 5 weeks of differentiation for further characterization. At this time point, the organoids consisted of NESCs organized into multiple pseudostratified VZ-like progenitor regions expressing SOX2 (Figures 1E). Cortical patterning was verified by co-expression of the dorsal telencephalon progenitor marker PAX6 (Georgala et al., 2011) in the VZ-like regions, which were surrounded by doublecortin (DCX)-positive neurons also expressing the deep-layer subcortical projection neuron marker CTIP2 (Molyneaux et al., 2005; Leone et al., 2008; Figure S2). Consistent with reduced organoid size, we found markedly increased apoptosis in the MDS cortical VZ-like regions, whereas the marker of proliferation was not significantly altered (Figures 1F–1H). Interestingly, although acute removal of *Pafah1b1* in the mouse telencephalon at embryonic day (E) 8-E8.5 leads to ESC apoptosis, genetic *Pafah1b1* heterozygosity does not exhibit a strong phenotype in the mouse neuroepithelium (Hirotsune et al., 1998; Yingling et al., 2008). Our results suggest that the human genetic model may be more sensitive in recapitulating lissencephaly severity and highlight an early defect in the founder population of neuroepithelial stem cells independent of neurogenesis or neuronal migration.

Increased Incidence of Horizontal Cleavage Angles in MDS Neuroepithelium at 5 Weeks

NESCs undergo interkinetic nuclear migration (INM) coordinately with the cell cycle and expand through symmetrical divisions with vertically oriented cleavage planes (60°–90° relative to the ventricular surface) at the apical VZ surface (Götz and Huttner, 2005). These cell-intrinsic properties, including apical-basal polarity, dynamic behavior, and precise regulation of mitotic spindle orientation, are recapitulated *in vitro* in cortical organoids (Movie S1; Kadoshima et al., 2013). We consistently found that both WT and MDS SOX1 and SOX2 ESC nuclei were distributed throughout the apical-basal VZ axis in a pseudo-stratified fashion, with mitotic cells expressing phospho-Vimentin and phospho-Histone H3 (Figures 2A and 2B), located at the apical surface. Other apical determinants, including α protein kinase C (α PKC), N-Cadherin, and Pericentrin, which marks the centrosomes, were generally localized at the apical surface in both genotypes (Figures 2A–2C). Notably, we sometimes observed a less organized cellular structure and a discontinuous VZ surface in MDS organoids (Figure 2B, right).

LIS1 and ASPM (a microcephaly causative gene) were shown to regulate mitotic spindle orientation in the developing mouse

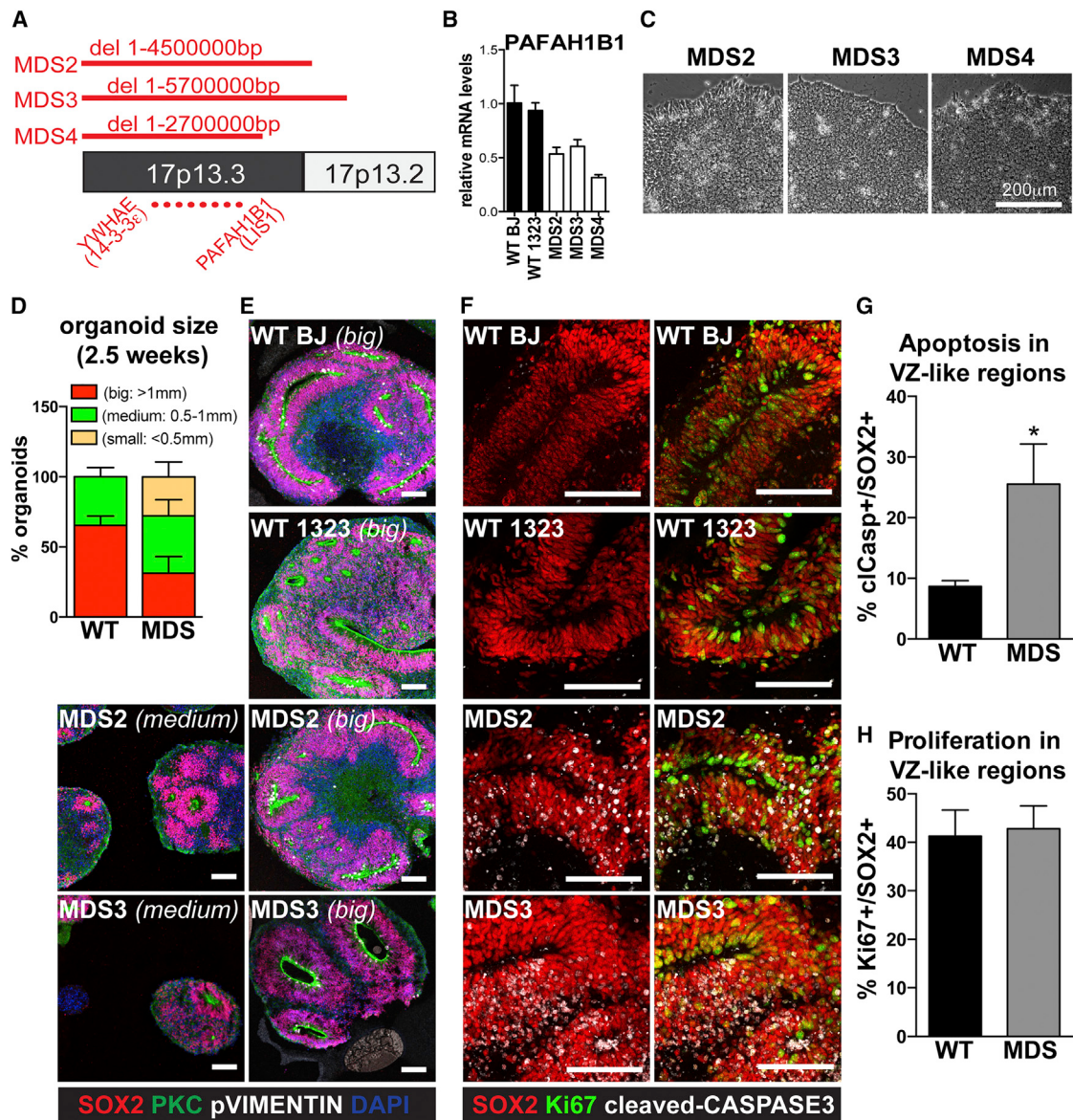


Figure 1. Apoptosis of NESCs in MDS Organoids

(A) Schematic and coordinates of the deletions (red lines) on chromosome 17 in MDS cells used in this study. The YWHAE and PAFAH1B1 genes delineate the minimal critical deletion that causes MDS.

(B) Quantitative real-time PCR analysis of PAFAH1B1 expression in the WT and MDS fibroblasts that were used to make iPSCs. Average values \pm SD for each individual are shown.

(C) Representative images of MDS iPSCs grown on Matrigel. Scale bar, 200 μ m.

(D) Analysis of organoid sizes at 2.5 weeks of differentiation, representing an average \pm SEM from WT ($n = 4$ independent iPSC clones) and MDS ($n = 6$ iPSC clones) (also see the table in STAR Methods).

(E) Representative images of organoid sections after 5 weeks of differentiation. Scale bar, 100 μ m.

(F) Representative images of VZ-like regions in 5-week organoids immunostained with the apoptotic marker cleaved CASPASE-3 (CASP3) and the proliferation marker Ki67. Scale bar, 100 μ m.

(G and H) Percent of SOX2 $^{+}$ cells in VZ-like regions expressing cleaved CASP3 (G) and Ki67 (H). Average values \pm SEM for WT ($n = 3$) and MDS ($n = 3$) are plotted (also see the table in STAR Methods). Statistical analysis was done using a t test ($p = 0.04$).

See also Figures S1 and S2 and Table S2.

forebrain, with loss of function leading to increased horizontal divisions associated with premature neurogenesis (Fish et al., 2006; Yingling et al., 2008; Pawlisz et al., 2008; Prampano et al., 2010; Xie et al., 2013). To determine whether a similar

defect is present in human lissencephaly, we analyzed mitotic cells in VZ-like regions of week 5 cortical organoids using time-lapse imaging (Figure 2C) and immunostaining (Figure 2D). In WT organoids, the majority of cleavage planes in the VZ were

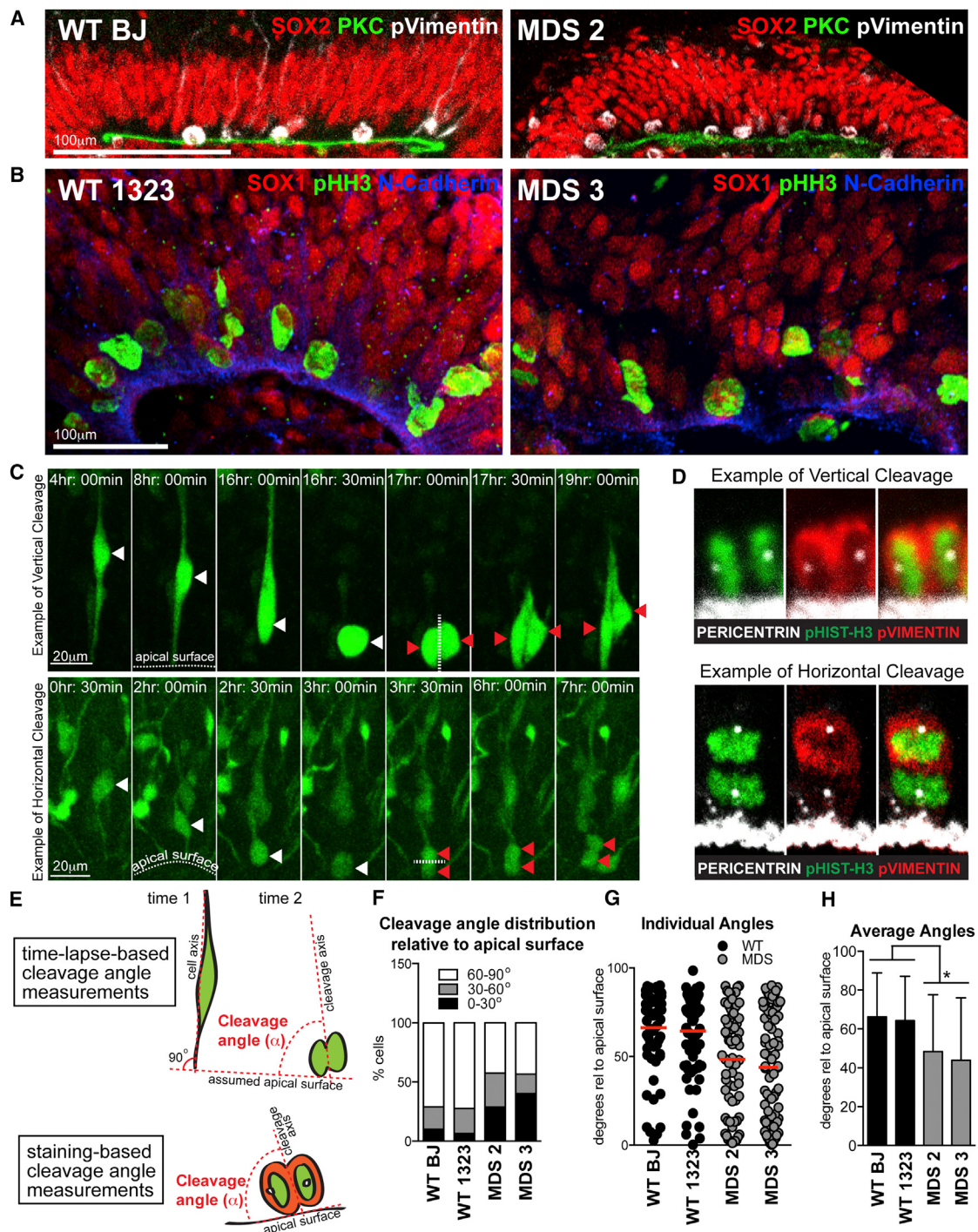


Figure 2. Increased Incidence of Horizontal Cleavage Angles in MDS VZ-like Regions at 5 Weeks

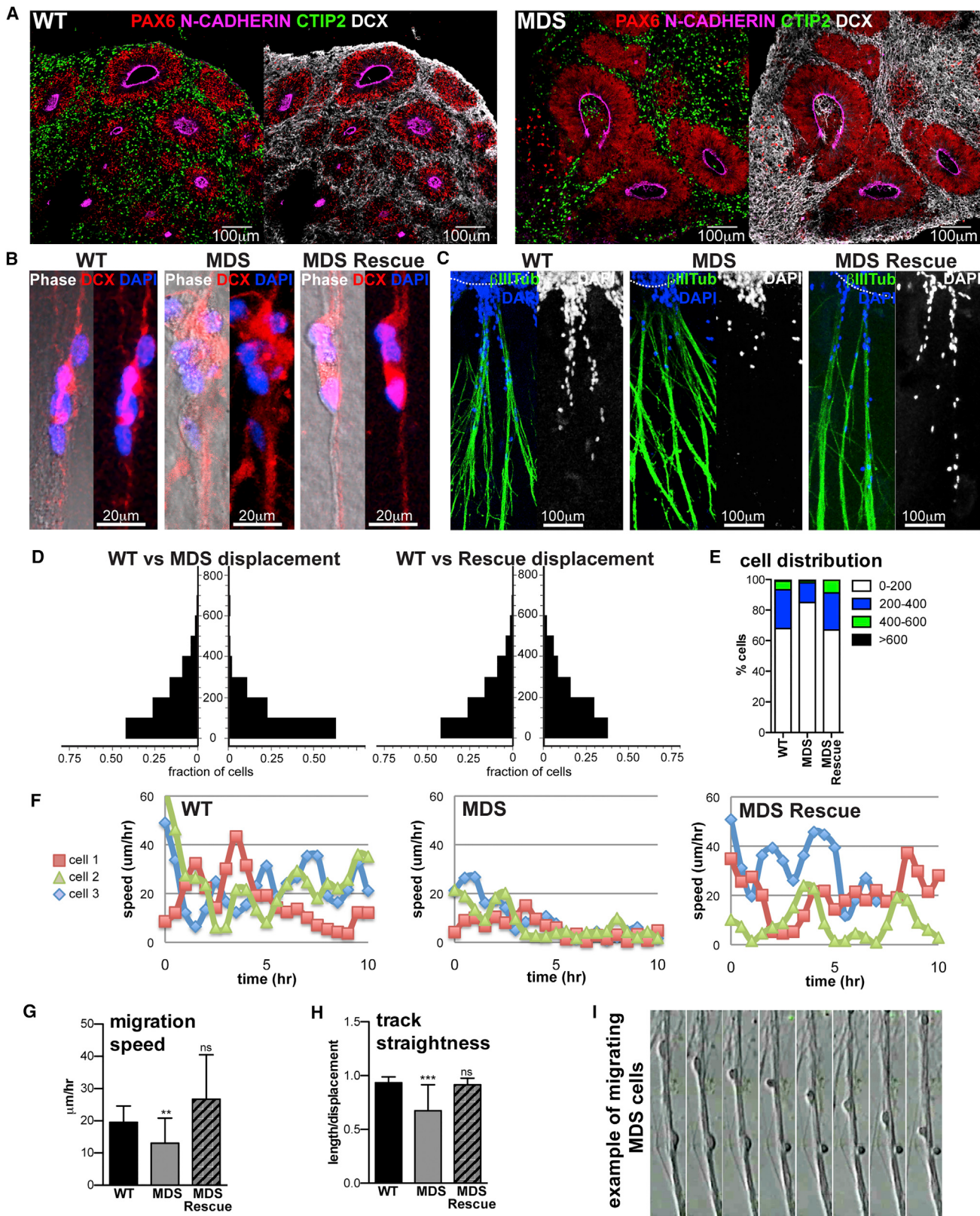
(A and B) Representative images of VZ-like regions in WT (left column) and MDS (right column). Scale bar, 100 μ m.

(C) Frames from time-lapse imaging showing examples of vertical (top) and horizontal (bottom) divisions. Scale bar, 20 μ m. White arrowheads mark the parent cell, and red arrowheads mark the progeny. The apical surface and the axis of the cleavage plane are demarcated with dotted white lines.

(D) Examples of vertical and horizontal divisions observed in VZ-like regions of fixed organoids. Anaphase mitoses were identified by chromosomal position and morphology; only anaphase cells were considered for analysis of the cleavage angle.

(E) Schematic of how cleavage angles were measured from time-lapse and immunostaining data.

(F–H) Quantification of cleavage angle data. Collectively, 70–92 dividing cells were analyzed from WT ($n = 2$) and MDS ($n = 2$) individuals. The red line in (G) represents the mean cleavage angle. Average cleavage angles \pm SD for each individual are shown (H). Statistical analysis was done using a t test ($p = 0.0158$). See also Movies S1 and S2 and Table S2.



(legend on next page)

perpendicular to the apical surface, with an average angle of ~65° (Figures 2E–2H). In contrast, dividing cells in the VZ regions of MDS organoids displayed more frequent horizontal cleavage planes and a significantly reduced average cleavage angle of ~46° (Figures 2E–2H; Movie S2). Collectively, our analyses suggest that expansion of the founder NESCs is greatly diminished in MDS because of increased apoptosis and decreased vertical divisions.

Defective Neuronal Migration in MDS Organoids at 5 Weeks

Defective radial migration of cortical neurons is a well-established developmental phenotype in lissencephaly (Hirotsume et al., 1998; Gambello et al., 2003; Youn et al., 2009; Toyo-oka et al., 2003; Sheen et al., 2006b; Saito et al., 2011). However, direct visualization and analysis of radial migration of human lissencephalic neurons have not been achieved. Thus, we sought to develop functional assays to analyze radial migration using the human organoid model system. Early-born subcortical projection neurons expressing CTIP2 and DCX were present by 5 weeks of differentiation (Figures S2 and 3A). Within a day of attachment to a Matrigel-coated surface, numerous processes began extending from the organoids. These processes were marked by expression of the neuronal proteins DCX and TUJ1 as well as the radial glia proteins BLBP and NESTIN (Figure S3), suggesting that they belong to bundles of neurites and radial glia fibers. The abundance and lengths of processes were comparable between WT and MDS organoids (Figure 3C; Figures S3A and S4D). Over the next 48 hr, DCX-positive neurons were observed migrating out of the organoids along these processes (Figures 3B and 3C; Figures S3 and S4D; Movie S3), akin to radial migration. We measured the displacement of neurons on fibers from the edge of the organoid 3 days after attachment to Matrigel. Migration of WT neurons was very robust, with more than 55% of migrating cells reaching 100–800 μm from the edge of the organoids (Figures 3C–3E; Figure S2A). In contrast, fewer MDS neurons migrated out of the organoids despite abundant processes, and the majority (65%) of migrating neurons were within 100 μm of the edge (Figures 3C–3E).

In addition to endpoint analyses, we tracked migrating neurons in real time using live imaging starting 1 day after organoid attachment for up to 48 hr. WT neurons migrated in a characteristic saltatory fashion (Figure 3F) with an average speed of 20 μm/hr (Figure 3G; Movie S3), comparable with what has been recorded during radial neuronal migration in ferret cortical

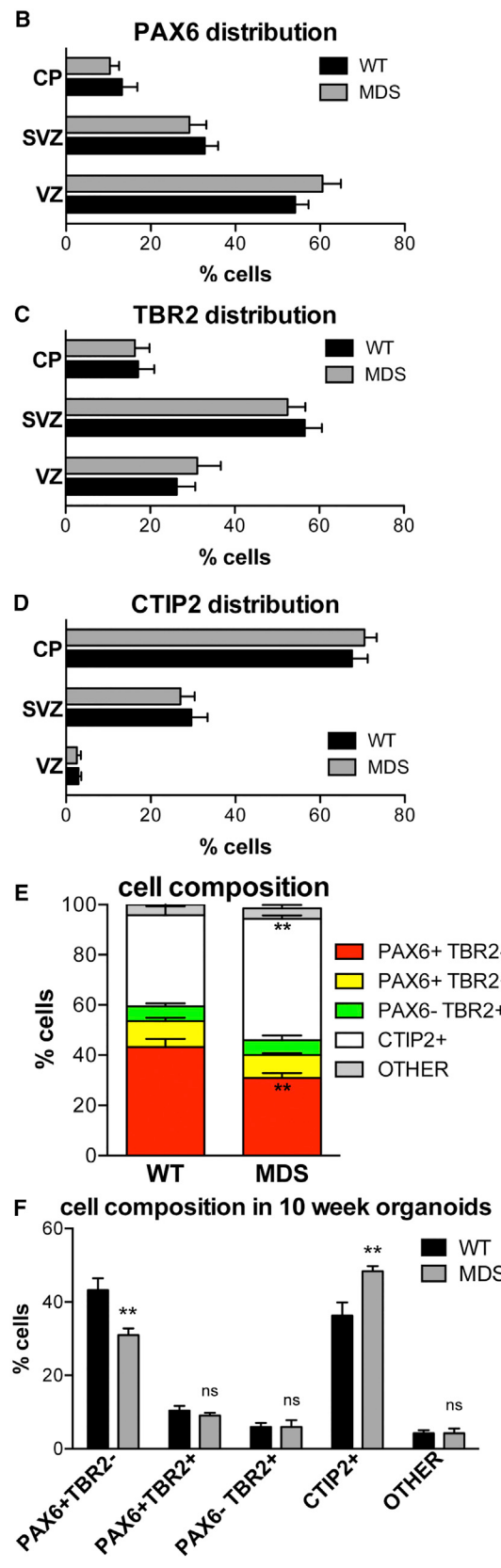
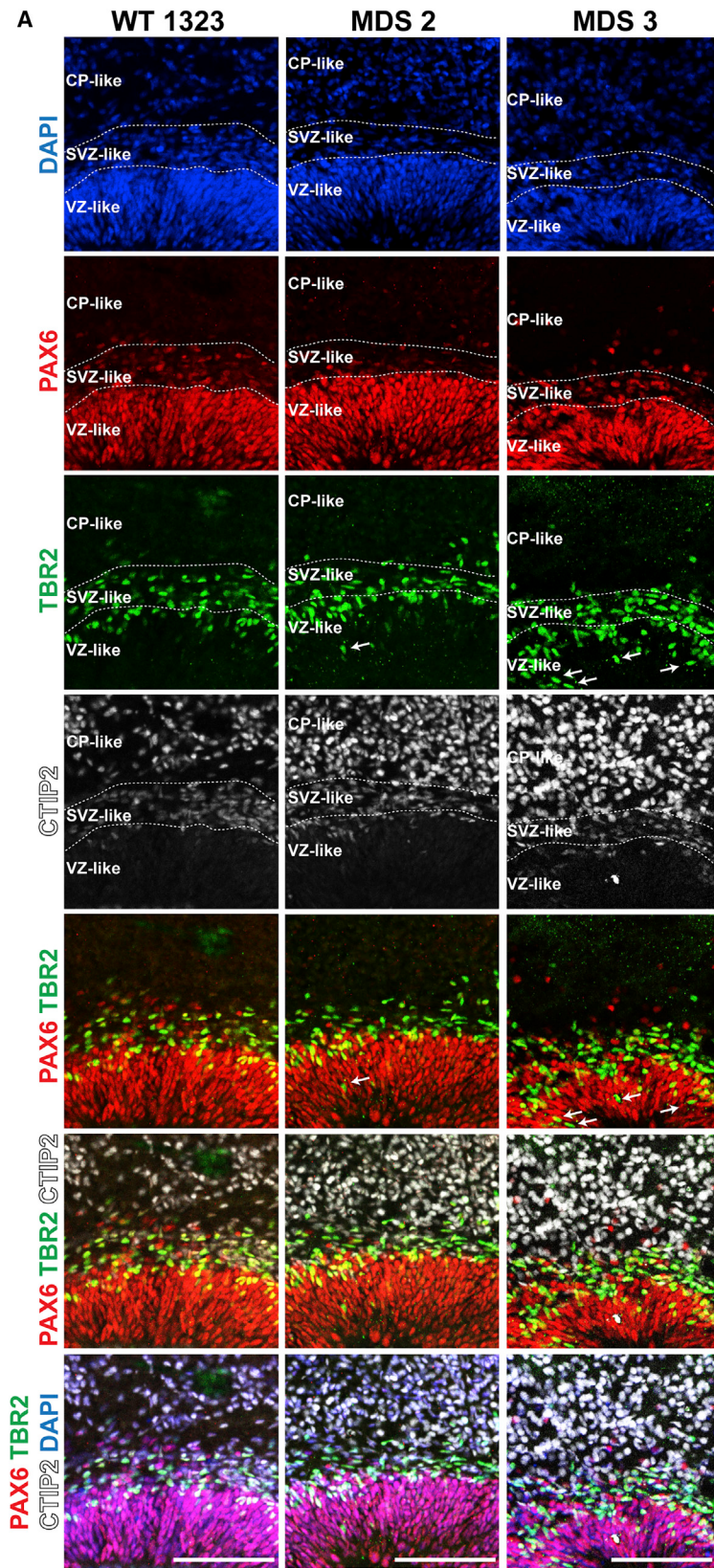
explants (Gertz and Kriegstein, 2015). In addition, WT neurons nearly always migrated away from the organoid along the processes. As a result, the calculated total length of the migratory track divided by the net displacement, or track straightness, was close to 1 for WT neurons (Figure 3H). In contrast, many of the MDS neurons initiated, but did not maintain, saltatory migration on processes, spending much of the time tumbling in place or not moving (Figures 3F and 3G; Movie S4), which significantly reduced the average migration speed (13 μm/hr, $p = 0.0004$) and track straightness (Figures 3G–3I). In addition, migrating MDS neurons had less elongated nuclei than WT neurons (Movie S4), consistent with reduced tension during nucleokinesis (Tanaka et al., 2004).

LIS1 and 14-3-3 ϵ proteins are part of a complex with cytoplasmic dynein that regulates neuronal migration (Toyo-oka et al., 2003). The corresponding genes, *PAFAH1B1* and *YWHAE*, are several megabases apart on locus 17p13.3 (Figure 1A) and would be challenging to rescue in MDS. However, we previously reported a reprogramming-induced rescue of an MDS case in which the 5.7-Mbp deletion affecting locus 17p13.3 was in a ring chromosome (Bershteyn et al., 2014). Upon reprogramming fibroblasts from this individual (MDS1), the ring was lost and replaced by a second copy of the wild-type chromosome 17 through compensatory uniparental isodisomy. As a consequence, the whole deletion was rescued in MDS1 iPSCs, and we showed that LIS1 and 14-3-3 ϵ proteins were restored to WT levels (Bershteyn et al., 2014). Remarkably, when we performed endpoint and live imaging-based migration assays with organoids from these iPSCs, we observed that MDS1 neurons were indistinguishable from the WT, completely rescuing neuronal displacement, migration speed, and track straightness (Figures 3C–3H; Movie S4).

Finally, to find out whether migration defects in MDS neurons are cell-autonomous, we developed a new assay using co-culture of organoids with human cortical tissue explants. Specifically, week 5 organoids were infected with a non-replicating, adeno-associated virus expressing td-Tomato fluorescent protein under the control of the CAG promoter (AAV1-cag-Tomato), which preferentially labels neurons (Figures S4A–S4D). About 60% of cells labeled with this virus expressed the neuronal marker CTIP2, and about 25% of the labeled cells expressed the progenitor marker SOX1, in both WT and MDS organoids (Figures S4B and S4C). Separately, slices of human cortical tissue (GW18.5) were infected with a cytomegalovirus (CMV)-GFP adenovirus and then placed tightly against the organoids to allow

Figure 3. Defective Neuronal Migration in MDS Is Rescued by Compensatory Duplication of Wild-Type Chromosome 17

- (A) Representative images of WT and MDS cortical organoids after 5 weeks of differentiation. Scale bar, 100 μm.
 - (B and C) Immunostaining of cells migrating on processes with DCX (B) and TUJ1 (C) 3 days after intact organoids were attached to Matrigel. Some of the processes seen in phase are not marked by DCX (B), suggesting that these may be radial glia fibers (see also Figure S3).
 - (D) Quantification of cell displacement along the processes on day 3. Shown on the y axis is distance from the edge of the organoid (micrometers), and shown on the x axis is the fraction of total migrating cells at the corresponding distance bin from WT (left side) and MDS or MDS rescue (right side) organoids. Migration assays were performed with WT ($n = 3$), MDS ($n = 3$), and MDS rescue ($n = 1$) individuals. Data from the third MDS individual are not represented in this quantification because there were very few (almost no) migrating cells (data not shown).
 - (E) Summary of cell distribution across 200-μm bins of displacement.
 - (F) Representative tracks of speed over time for three different WT, MDS, and MDS rescue cells.
 - (G and H) Migration speed (G) and track straightness (H). Average ± SD is plotted.
 - (I) Frames from time-lapse imaging of an MDS sample, showing two cells migrating on processes. The top cell exhibits a saltatory migration pattern of rounding up, followed by leading process extension, whereas the bottom cell rounds up but fails to continue migration.
- See also Figures S3 and S4, Movies S3 and S4, and Table S2.



(legend on next page)

attachment of the differentially labeled tissues. The human cortical tissue thus provided a physiological substrate for migration of iPSC-derived neurons (Figure S4E). After 4 days of co-culture, Tomato-expressing cells from the organoids were found throughout the cortical tissue explants, and their position relative to the ventricular and pial surfaces was quantified. Fifty percent of the WT iPSC-derived neurons that migrated had reached the pial surface after 4 days (Figure S4G). In contrast, only about 10% of the MDS iPSC-derived neurons that migrated had reached the pial surface on the cortical tissue explants (Figure S4G), suggesting that MDS migration defects are cell-autonomous. Collectively, we established two novel *in vitro* migration assays that are sensitive to defects associated with human lissencephaly and can be used *in vitro* to study multiple dynamic aspects of neuronal migration. Moreover, we demonstrated that this major developmental phenotype in MDS is functionally rescued through the duplication of the wild-type homolog of chromosome 17, confirming that the migration defects were due to the heterozygous deletion.

Normal Lamination with Increased Abundance of Deep-Layer Neurons in MDS Organoids at 10 Weeks

Although the long-term consequence of increased horizontal divisions is expected to be a reduction in total neuronal output through depletion of the progenitor pool (Pawlisz et al., 2008), the short-term consequence might be the opposite; i.e., overproduction of neurons. To examine this, we analyzed the distribution of progenitor cells and neurons in 10-week cortical organoids. At this time point, staining with the RG marker PAX6, the IP cell marker TBR2/EOMES (eomesodermin) (Hevner et al., 2006), and the deep-layer cortical neuron marker CTIP2 revealed three distinct regions resembling the developing VZ, SVZ, and cortical plate (CP). The boundaries between these regions could be consistently demarcated in WT and MDS organoids based on cell density, cell orientation, and expression of the three transcription factors. Thus, the VZ was defined based on dense vertical columns of PAX6-positive RG cells (Figure 4A). The SVZ was defined based on less dense, horizontally oriented cells, many of which expressed TBR2 (Figure 4A). Immediately superficial to the TBR2 boundary was the rudimentary CP, with strong expression of CTIP2 (Figure 4A). These well-organized structures were found close to the surface in every cortical organoid (typically one to five per organoid), with neurons always found on the outside, superficial to the progenitors.

We analyzed the distribution of the PAX6-, TBR2-, and CTIP2-expressing cell populations in at least 12 organoids from WT ($n = 3$) and MDS ($n = 2$) individuals generated in multiple independent differentiations. The distribution of PAX6, TBR2, and CTIP2

was not significantly different between the two genotypes, with the majority of PAX6⁺ cells (~60%) found in the VZ, the majority of TBR2⁺ cells (~55%) in the SVZ, and the majority of CTIP2⁺ cells (~70%) in the CP, as expected (Figures 4B–4D), indicating that the general laminar distribution of cell types is preserved. However, in MDS organoids, particularly in the more severe MDS3 case, there was a notable increase in the abundance of IP cells located in the apical portions of the VZ (arrows in Figure 4A). In addition, analysis of relative cell proportions in the organized cortical regions revealed a slight but significant decrease in PAX6⁺/TBR2⁻ RG cells with a complementary increase in CTIP2⁺ neurons in MDS (Figures 4A, 4E, and 4F). These findings are consistent with the increase in horizontal divisions we observed at earlier time points in MDS organoids and indicate an overproduction of deep-layer neurons. Moreover, these data indicate that migration defects are not likely to be a secondary consequence of neuronal deficiency because no such deficiency was observed up to this point.

Histological and Molecular Evidence of oRG-like Cell Production in WT and MDS Organoids after 10 Weeks

By 10 weeks, close to 30% of PAX6-positive cells within organized structures were located in the SVZ-like regions (Figures 4A and 4B) and expressed other canonical radial glia genes such as SOX2 and SOX1 (Figure 5A and data not shown). We sought to determine whether some of these cells might be oRGs. In contrast to the ventricular or apical radial glia (vRG/aRG), which extend bipolar processes and attach to the ventricular surface (Florio and Huttner, 2014), oRG cells reside in the SVZ and are typically unipolar, extending a single basal process toward the pial surface (Hansen et al., 2010; Fietz et al., 2010). After 10–15 weeks of culture, the outer edge of the organoids contained many radially oriented cells with unipolar processes pointing away from the center of the organoids (white arrows in Figures 5B; Figure S5A). Many of these unipolar cells expressed the radial glia marker SOX2 (Figure 5C; Figure S5A), consistent with oRG identity. Within the same regions, IP-like cells with characteristic multipolar morphologies and expression of TBR2/EOMES could be clearly distinguished from oRG-like cells (blue arrow in Figure S5A).

A recent study used transcriptome-wide profiling of single cells to show that stem cell-derived cerebral organoids can recapitulate many of the molecular pathways that control normal human cortical neurogenesis (Camp et al., 2015). We reasoned that a subset of radial glia derived *in vitro* may adopt the molecular profile of oRG cells. Therefore, we analyzed single-cell gene expression from WT and MDS organoids after 5, 10, and 15 weeks of differentiation. We identified a group of 95 cortical

Figure 4. Increased Abundance of CTIP2-Positive Neurons in MDS Organoids at 10 Weeks

(A) Representative images of WT (1323), MDS2, and MDS3 cortical organoids. Scale bar, 100 μ m. The inferred VZ-, SVZ-, and CP-like regions are delineated based on the combination of DAPI, PAX6, TBR2, and CTIP2 staining patterns. White arrows in the MDS TBR2 and PAX6/TBR2 panels point to IP cells located in the apical portions of the VZ. (B–F) Analysis of marker distribution across the VZ/SVZ/CP (B–D) and cell composition (E and F) within the organized regions in WT (12 total organoids from 3 individuals, 4 iPSC clones) and MDS (13 organoids from 2 individuals, 3 iPSC clones) organoids. The average value \pm SEM is plotted after collapsing technical replicates from each clone (WT, $n = 4$; MDS, $n = 3$). Two-way ANOVA followed by Bonferroni's adjustment for multiple comparisons was performed to determine statistical significance. For cell distribution (B and C), the only significant source of variation was region. For cell composition, there was a significant difference between WT and MDS in the proportion of PAX6⁺TBR2⁻ cells and CTIP2⁺ cells.

See also Table S2.

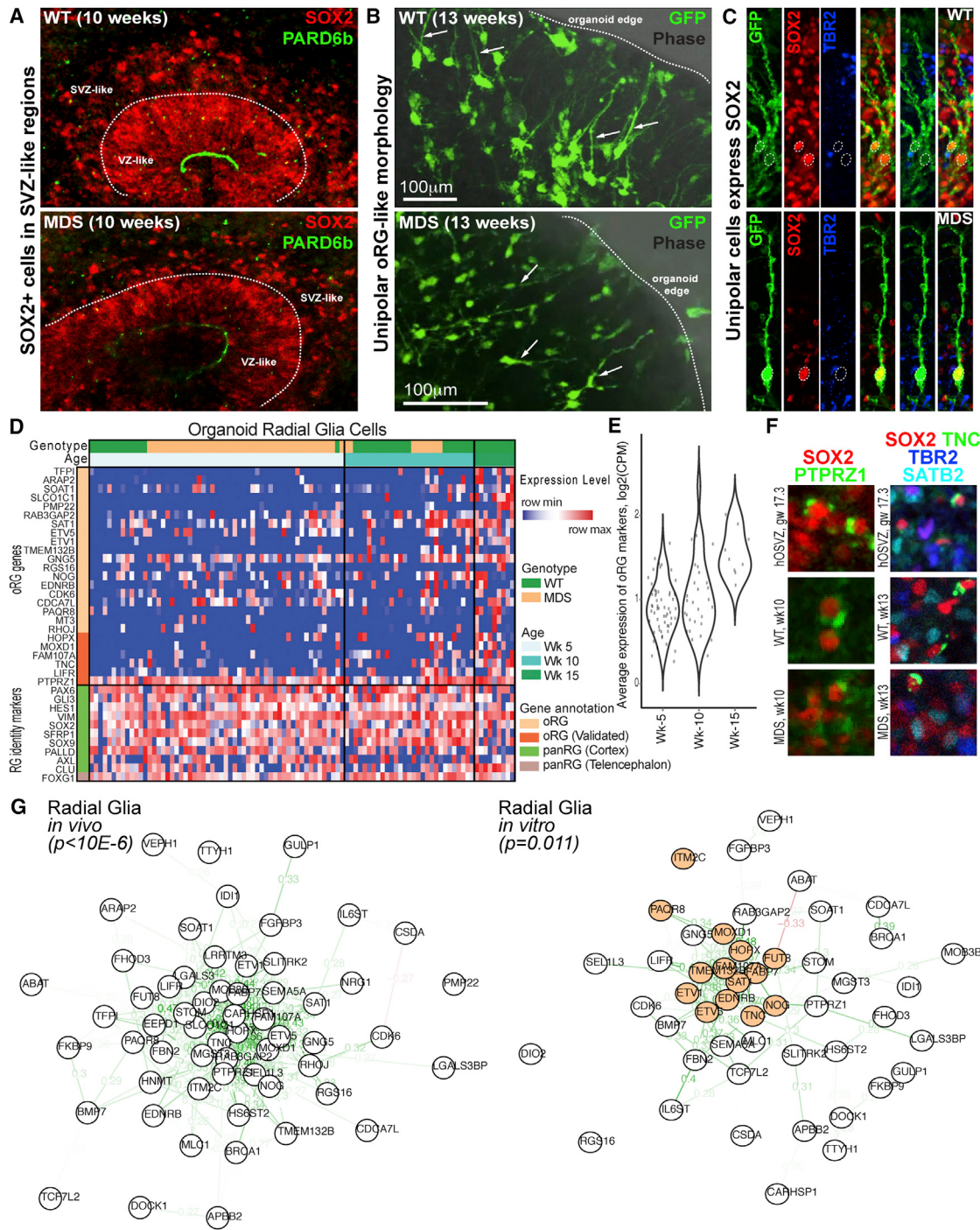


Figure 5. Production of oRG Cells in Organoids after 10 Weeks

(A) Representative images of WT and MDS progenitor zones in 10-week organoids.

(B) GFP labeling with adenovirus reveals unipolar morphology and radial orientation of cells close to the edge of the organoids. Scale bar, 100 μ m.

(C) Immunostaining confirms radial glia fate of unipolar cells that express SOX2 and not the IP cell marker TBR2.

(D) Heatmap showing relative gene expression levels across 95 single radial glia cells captured from cerebral organoid samples ($n = 5$ individuals from both WT and MDS). Genes represent canonical markers of radial glia (green bar) and forebrain identity (brown bar) as well as genes correlated with oRG identity (light and dark orange; the dark shade highlights genes validated in vivo) (Pollen et al., 2015). The expression of oRG-correlated genes increases with age of the organoid (also see Figure S5).

(E) Violin plots representing distribution of the average expression of oRG marker genes across single cells captured from cerebral organoids at each stage of differentiation.

(legend continued on next page)

radial glia-like cells (Figure 5D) out of all the in vitro-derived cells (Figure S6A; see STAR Methods for clustering methods). Among these radial glia-like cells, we found that the oRG gene expression signature (Pollen et al., 2015) emerged at week 10 and became stronger at week 15 (Figure 5E; Figures S6B and S6C), consistent with observations from histology. We confirmed the expression of a few oRG markers in a subset of organoid radial glia that showed consistent subcellular localization to human tissue (Figure 5F). In addition, the expression of many of the predicted and validated oRG markers is well correlated across radial glia-like cells from organoids, indicating that these genes are also co-expressed in the in vitro system (Figure 5G). Together, these data establish the presence of oRG-like cells that share features of tissue-level distribution, morphology, and molecular identity with oRG cells found in the developing human cortex.

oRG Cell-Specific Cytokinesis Delay in Human Lissencephaly

The ability to recapitulate human oRG production and 3D organization in vitro enabled us to analyze the effect of lissencephaly mutations on this class of progenitors. Toward that end, we performed time-lapse imaging following infection of 10-week organoids with CMV-GFP adenovirus, which labels all dividing progenitors including vRG, IP, and oRG cells. The morphology, spatial organization, and mitotic behavior of GFP-labeled progenitors were consistent with properties observed in vivo. IP-like cells had a larger cell body with multiple short processes (blue arrows in Figure 6A and Figure S5A), and they divided in place without much movement (Figure S5B). vRG cells were typically bipolar, with apical processes coalescing at a common VZ-like surface, and their nuclei underwent apically oriented INM prior to division at the apical surface (arrowheads in Figures 6A, 1 and 2, and 6D). In contrast, oRG cells had a single long basal process and a very short apical process, were located above the ventricular-like zone (stars in Figure 6A, 1, and Figure S5C), and underwent a rapid mitotic somal translocation (MST) in the direction of the basal process prior to division (Figure 6G; Movie S5).

To examine whether MDS mutations affect the behavior of vRG and oRG cells, we measured multiple dynamic properties. For both vRG and oRG cells, we measured the *time* from when the dividing cell was rounded up to when the two daughters first appeared and the *angle* of the cleavage plane relative to the basal fiber (Figures 6B and 6C). In addition, we measured MST *distance* for oRG cells (Figure 6C). We found that WT oRG and vRG cells divided within 50 min from the time that the cell rounded up (Figures 6D, 6F, 6G, and 6J; Movie S5). Surprisingly, MDS oRG cells tended to translocate farther during MST (Figure 6K) but then remained in mitosis for prolonged periods (up to several hours) prior to cytokinesis (Figures 6H and 6J; Figure S5C; Movie S5). The delay in cell division appeared to be

specific to MDS oRG cells because a similar defect was not observed in vRG or IP cell divisions from the same imaging sessions (Figures 6E and 6F; Figure S5B). Of note, this behavior mimicked a phenotype previously observed in primary oRG cells treated with a microtubule-depolymerizing agent, nocodazole (Ostrem et al., 2014). We also compared the division cleavage angle relative to the basal process in dividing vRG and oRG cells between WT and MDS groups using live imaging. This analysis confirmed in vivo observations that vRG divisions become less tightly controlled with developmental maturation and that the majority of oRG divisions occur perpendicular to the basal process (Figures 6L and 6M; LaMonica et al., 2013). There were no significant differences between the two genotypes in terms of division cleavage angles (Figures 6K and 6L). Collectively, our findings implicate MDS-deleted genes in the regulation of oRG cell division and point to a possible involvement of oRG cells in the pathogenesis of human lissencephaly.

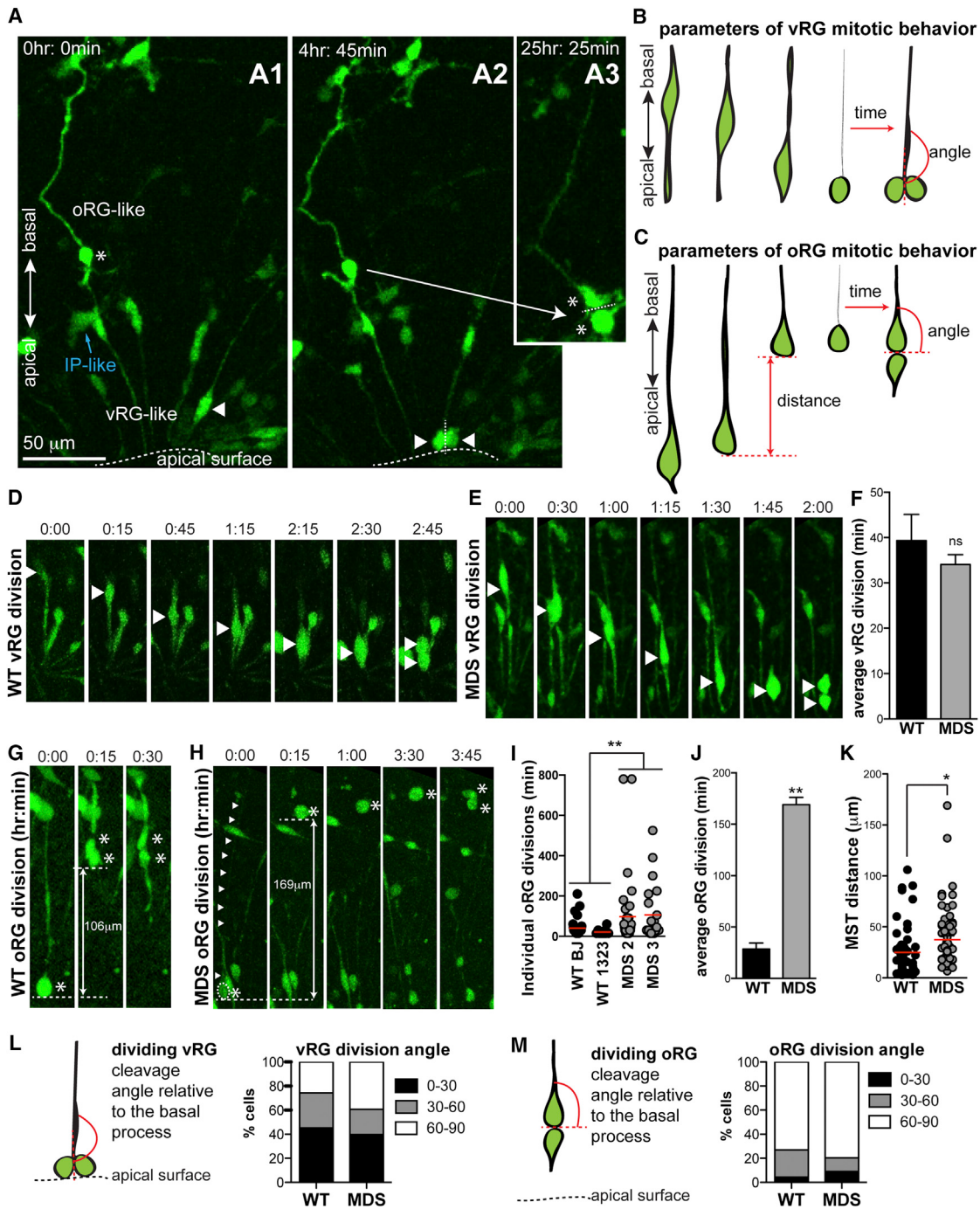
DISCUSSION

By implementing a patient iPSC-derived 3D model of early corticogenesis, we were able to delineate cell type- and cell stage-specific defects in human lissencephaly caused by deletions of the distal tip of chromosome 17. Ultimately, these defects need to be linked with the corresponding genetic regulators for a deeper understanding of lissencephaly pathogenesis and human cortical development. Although *Pafah1b1* (LIS1) and *YWHAE* (14-3-3 ϵ) mutations have been modeled in the rodent (Hirotsune et al., 1998; Toyo-oka et al., 2003; Gambello et al., 2003; Youn et al., 2009), there has been a lack of laboratory models that recapitulate the complete genetic defects of MDS. Thus, the roles of most of the deleted genes in brain development or MDS pathogenesis have not been examined. Here we provide a platform and establish functional assays that will enable validation of additional gene candidates in distinct cell types and cellular processes and will lead to identification of novel regulators of cortical development and malformation.

Several of the conserved developmental phenotypes implicated in lissencephaly by mouse models, including dysregulation of the NESC mitotic spindle (Faulkner et al., 2000; Yingling et al., 2008; Pawlisz et al., 2008; Pramparo et al., 2010; Xie et al., 2013; Moon et al., 2014) and neuronal migration defects (Hirotsune et al., 1998; Gambello et al., 2003; Youn et al., 2009; Toyo-oka et al., 2003) are recapitulated here. Deficiencies in neural progenitor cell viability in human MDS were previously implicated by Sheen et al. (2006a) based on the analysis of post-mortem samples but without distinguishing which progenitor subclasses were affected. Here, by following in vitro differentiation from patient-derived iPSCs, we were able to recapitulate developmental lineage progression from NESCs to vRG to IP and oRG with spatial and temporal resolution that could not have been achieved with previous methods. Our analyses

(F) Validation of oRG marker (PTPRZ1 and tenascin C [TNC]) co-expression with the radial glia marker SOX2 in 10-week organoids. Note the similarity in the staining pattern between human OSVZ (GW17.3) and iPSC-derived organoids.

(G) Network maps representing Pearson's correlation between oRG marker genes across single cells in primary human brain tissue (Pollen et al., 2015) (left) and across cells captured from cerebral organoids (right). Correlations greater than 0.25 are highlighted with a pale green line, and correlations greater than 0.5 are highlighted with a dark green line. Genes that are most highly correlated across in vitro cells out of the oRG marker genes are highlighted in orange. See also Figures S5 and S6, Tables S1 and S2, and dbGaP: phs000989.v3.p1.

**Figure 6. Prolonged Mitosis in MDS oRG, but Not vRG, Cells at 10 Weeks**

(A) Frames from time-lapse imaging showing representative examples of distinct vRG and oRG cell morphology, orientation, and dividing properties in the same imaging field. The oRG-like cell is marked with a white star. Note the long basal process and its superficial location relative to the bipolar vRG-like cells (example: white arrowhead). The indicated bipolar vRG-like cell from A1 moves apically and divides in A2 with a cleavage angle parallel to its basal process. In contrast, the indicated oRG-like cell undergoes an MST in the basal direction (data not shown) and divides in A3 with a cleavage angle perpendicular to its basal process. Scale bar, 50 μ m.

(B) Schematic of parameters used to analyze vRG mitotic behavior: time from cell rounding to the first appearance of two daughters and angle of cleavage relative to the cell body axis just prior to basal process retraction.

(C) Schematic of parameters used to analyze oRG mitotic behavior: MST distance, time from cell rounding to the first appearance of two daughters, and angle of cleavage relative to the basal process.

(D and E) Frames from time-lapse imaging showing representative examples of WT (D) and MDS (E) vRG-like divisions.

(F) Quantification of vRG divisions.

(legend continued on next page)

suggest that founder NESCs and oRG cells are particularly vulnerable in MDS, whereas vRG and IP cells seem to be less affected.

Outer RG progenitors are thought to support the developmental and evolutionary expansion of the human neocortex because of their tremendous proliferative potential (Lukaszewicz et al., 2005; Hansen et al., 2010; Fietz et al., 2010; Pollen et al., 2015). In addition, oRG cells have been proposed to promote cortical folding by producing large numbers of neurons and by providing divergent tracks for increased tangential dispersion of migrating neurons along their basal fibers (Lui et al., 2011; Fietz and Huttner, 2011; Hevner and Haydar, 2012; Florio and Huttner, 2014; Taverna et al., 2014; Borrell and Götz, 2014; Nowakowski et al., 2016a). Our studies identified specific mitotic defects in oRG cells from a severe form of lissencephaly, providing another link between this cell type and human neocortical gyration.

Prolonged mitosis of mouse cortical radial glia in a *Magoh*^{+/−} model of microcephaly was recently shown to induce preferential production of neurons rather than progenitors as well as increased incidence of apoptotic progeny (Pilaz et al., 2016). Mitotic delay through pharmacological means also altered cell fate, producing more apoptotic progeny or leading to ectopic neuronal differentiation. Similarly to Pilaz et al. (2016), we observed examples of apoptotic oRG-like cells (data not shown); however, the technical challenges of prolonged time-lapse imaging of organoid slices precluded us from direct visualization of progeny fate. Interestingly, *Magoh* functions upstream of *Pafah1b1*, with loss of function leading to decreased LIS1 protein levels during neurogenesis (Silver et al., 2010). This connection suggests a possible mechanistic basis for the convergence of microcephaly and lissencephaly phenotypes in MDS.

The genetic factors that regulate oRG behavior have been difficult to study because of the scarcity of these cells in mice. Here we find that cerebral organoids generate oRG-like cells with matching properties defined in vivo, including position, morphology, mitotic behavior, and molecular identity. In addition, we show that the DNA sequence in the MDS deletion interval is necessary for normal MST behavior. MDS oRG cells exhibited increased MST distance, similar to the effect of nocodazole (Ostrem et al., 2014), which interferes with microtubule cytoskeleton polymerization. Among the deleted genes, *PAFAH1B1* is known to control microtubule dynamics during mitosis (Yingling et al., 2008; Moon et al., 2014), pointing to a possible oRG-specific regulatory mechanism that may be LIS1-dependent. However, LIS1 haploinsufficiency alone cannot account for the severity of MDS because mutations or smaller deletions affecting only *Pafah1b1* have less severe outcomes and are not associated with human microcephaly (Ledbetter et al., 1992; Lo Nigro et al., 1997; Pilz et al., 1998; Barkovich et al., 1991; Cardoso et al., 2003). Therefore, additional genes in the MDS-deleted locus are likely involved in

the regulation of oRG cell division. Future studies can examine the role of specific candidate genes in this interval using the organoid model system, which recapitulates key features of oRG biology.

Finally, the involvement of oRG cells in the pathophysiology of MDS suggests a link between this radial glial subtype and the development of lissencephaly. In addition to genetic causes, cortical abnormalities, including lissencephaly and microcephaly, may also result from infectious diseases, including cytomegalovirus (CMV) and West Nile virus (Lanari et al., 2012; Teissier et al., 2014; O’Leary et al., 2006). Recently, Zika virus has been declared a public health emergency of international concern (Heymann et al., 2016) because of a strong correlation with increased incidence of microcephaly, which has been reported to involve lissencephaly (Oliveira Melo et al., 2016; Schuler-Faccini et al., 2016; Mlakar et al., 2016). These infectious diseases may preferentially affect the same cell types and developmental process that are vulnerable in genetic forms of microcephaly and lissencephaly. The Zika virus can infect human cortical neural progenitors, leading to cell death and cell cycle dysregulation (Tang et al., 2016; Qian et al., 2016) and has been shown to infect human skin cells through the phosphatidylserine receptor AXL (Hamel et al., 2015). We have found that radial glia cells show very high expression of the candidate Zika virus entry factor AXL (Nowakowski et al., 2016b), and the current study highlights how stalled mitosis of oRG cells may relate to lissencephaly. Collectively, these observations support the hypothesis that oRG dysfunction may be a feature of cortical malformations associated with lissencephaly.

STAR METHODS

Detailed methods are provided in the online version of this paper and include the following:

- KEY RESOURCES TABLE
- CONTACT FOR REAGENT AND RESOURCE SHARING
- EXPERIMENTAL MODEL AND SUBJECT DETAILS
 - hiPSC derivation and culture methods
- METHOD DETAILS
 - Cerebral organoid generation and culture
 - Quantitative PCR (qPCR)
 - Organoid slice culture, viral infection and time-lapse imaging
 - Neuronal migration assays
 - Immunocytochemistry
 - Single Cell RNA-Sequencing
 - Outlier removal and enrichment for cortical lineage cells
 - Identification of radial glia-like cells and analysis of heterogeneity

(G and H) Frames from time-lapse imaging showing representative examples of WT (G) and MDS (H) oRG-like divisions.

(I and J) Quantification of oRG division time showing individual events (I) and average values for each genotype (J) ($p = 0.0028$).

(K) Quantification of oRG MST distance ($p = 0.05$).

(L and M) Schematic and quantification of vRG (L) and oRG (M) cleavage angle relative to the basal process.

Average values \pm SEM are plotted in (F) and (J). Statistical analysis was done using a t test (WT, $n = 3$; MDS, $n = 2$). For all phenotypes, 20–50 cells were analyzed from each individual. See also Figure S5, Movie S5, and Table S2.

- QUANTIFICATION AND STATISTICAL ANALYSIS
- DATA AND SOFTWARE AVAILABILITY
 - Data Resources

SUPPLEMENTAL INFORMATION

Supplemental Information includes six figures, two tables, and five movies and can be found with this article online at <http://dx.doi.org/10.1016/j.stem.2016.12.007>.

AUTHOR CONTRIBUTIONS

M.B. conceived the project with guidance from A.W.B. and A.R.K. All experiments were designed and performed by M.B. with help from E.D.L. and A.N. Single-cell capture was performed by M.B. and T.J.N. RNA sequencing data analysis was performed by T.J.N. and A.A.P. M.B. prepared the figures and wrote the manuscript with input from all authors.

ACKNOWLEDGMENTS

The authors are grateful to Joseph Loturco, Catherine Priest, Haim Belinson, Carmen Sandoval Espinosa, and members of the A.R.K. and A.W.B. labs for helpful feedback on the manuscript. We thank Melanie Bedolli, Lillian Adame, and Yingling Wang for technical support. M.B. was supported by a postdoctoral fellowship from the California Institute for Regenerative Medicine, CIRM (Grant TG2-01153), and a K99 career development award from the National Institute for Neurological Disorders and Stroke (Grant 5K99NS088572). This research was funded by NIH Grants NS075998 and MH105989 and CIRM Award GCIR-06673 (to A.R.K.).

Received: July 8, 2016

Revised: October 16, 2016

Accepted: December 16, 2016

Published: January 19, 2017

REFERENCES

- Armstrong, E., Schleicher, A., Omran, H., Curtis, M., and Zilles, K. (1995). The ontogeny of human gyration. *Cereb. Cortex* 5, 56–63.
- Barkovich, A.J., Koch, T.K., and Carroll, C.L. (1991). The spectrum of lissencephaly: report of ten patients analyzed by magnetic resonance imaging. *Ann. Neurol.* 30, 139–146.
- Bershteyn, M., Hayashi, Y., Desachy, G., Hsiao, E.C., Sami, S., Tsang, K.M., Weiss, L.A., Kriegstein, A.R., Yamanaka, S., and Wynshaw-Boris, A. (2014). Cell-autonomous correction of ring chromosomes in human induced pluripotent stem cells. *Nature* 507, 99–103.
- Betizeau, M., Cortay, V., Patti, D., Pfister, S., Gautier, E., Bellemin-Ménard, A., Afanassieff, M., Huissoud, C., Douglas, R.J., Kennedy, H., and Dehay, C. (2013). Precursor diversity and complexity of lineage relationships in the outer subventricular zone of the primate. *Neuron* 80, 442–457.
- Borrell, V., and Götz, M. (2014). Role of radial glial cells in cerebral cortex folding. *Curr. Opin. Neurobiol.* 27, 39–46.
- Camp, J.G., Badsha, F., Florio, M., Kanton, S., Gerber, T., Wilsch-Bräuninger, M., Lewitus, E., Sykes, A., Hevers, W., Lancaster, M., et al. (2015). Human cerebral organoids recapitulate gene expression programs of fetal neocortex development. *Proc. Natl. Acad. Sci. USA* 112, 15672–15677.
- Cardoso, C., Leventer, R.J., Ward, H.L., Toyo-Oka, K., Chung, J., Gross, A., Martin, C.L., Allanson, J., Pilz, D.T., Olney, A.H., et al. (2003). Refinement of a 400-kb critical region allows genotypic differentiation between isolated lissencephaly, Miller-Dieker syndrome, and other phenotypes secondary to deletions of 17p13.3. *Am. J. Hum. Genet.* 72, 918–930.
- Chi, J.G., Dooling, E.C., and Gilles, F.H. (1977). Gyral development of the human brain. *Ann. Neurol.* 1, 86–93.
- Chong, S.S., Pack, S.D., Roschke, A.V., Tanigami, A., Carrozzo, R., Smith, A.C.M., Dobyns, W.B., and Ledbetter, D.H. (1997). A revision of the lissencephaly and Miller-Dieker syndrome critical regions in chromosome 17p13.3. *Hum. Mol. Genet.* 6, 147–155.
- Dobyns, W.B., Stratton, R.F., Parke, J.T., Greenberg, F., Nussbaum, R.L., and Ledbetter, D.H. (1983). Miller-Dieker syndrome: Lissencephaly and monosomy 17p. *J. Pediatr.* 102, 552–558.
- Dobyns, W.B., Curry, C.J.R., Hoyme, H.E., Burlington, L., and Ledbetter, D.H. (1991). Clinical and molecular diagnosis of Miller-Dieker syndrome. *Am. J. Hum. Genet.* 48, 584–594.
- Eiraku, M., Watanabe, K., Matsuo-Tasaki, M., Kawada, M., Yonemura, S., Matsumura, M., Wataya, T., Nishiyama, A., Muguruma, K., and Sasai, Y. (2008). Self-organized formation of polarized cortical tissues from ESCs and its active manipulation by extrinsic signals. *Cell Stem Cell* 3, 519–532.
- Faulkner, N.E., Dujardin, D.L., Tai, C.Y., Vaughan, K.T., O'Connell, C.B., Wang, Y., and Vallee, R.B. (2000). A role for the lissencephaly gene LIS1 in mitosis and cytoplasmic dynein function. *Nat. Cell Biol.* 2, 784–791.
- Fietz, S.A., and Huttner, W.B. (2011). Cortical progenitor expansion, self-renewal and neurogenesis—a polarized perspective. *Curr. Opin. Neurobiol.* 21, 23–35.
- Fietz, S.A., Kelava, I., Vogt, J., Wilsch-Bräuninger, M., Stenzel, D., Fish, J.L., Corbeil, D., Riehn, A., Distler, W., Nitsch, R., and Huttner, W.B. (2010). OSVZ progenitors of human and ferret neocortex are epithelial-like and expand by integrin signaling. *Nat. Neurosci.* 13, 690–699.
- Fish, J.L., Kosodo, Y., Enard, W., Pääbo, S., and Huttner, W.B. (2006). Aspm specifically maintains symmetric proliferative divisions of neuroepithelial cells. *Proc. Natl. Acad. Sci. USA* 103, 10438–10443.
- Florio, M., and Huttner, W.B. (2014). Neural progenitors, neurogenesis and the evolution of the neocortex. *Development* 141, 2182–2194.
- Gambello, M.J., Darling, D.L., Yingling, J., Tanaka, T., Gleeson, J.G., and Wynshaw-Boris, A. (2003). Multiple dose-dependent effects of Lis1 on cerebrum cortical development. *J. Neurosci.* 23, 1719–1729.
- Gaspard, N., Bouschet, T., Hourez, R., Dimidschstein, J., Naeije, G., van den Ameele, J., Espuny-Camacho, I., Herpoel, A., Passante, L., Schiffmann, S.N., et al. (2008). An intrinsic mechanism of corticogenesis from embryonic stem cells. *Nature* 455, 351–357.
- Georgala, P.A., Carr, C.B., and Price, D.J. (2011). The role of Pax6 in forebrain development. *Dev. Neurobiol.* 71, 690–709.
- Gertz, C.C., and Kriegstein, A.R. (2015). Neuronal Migration Dynamics in the Developing Ferret Cortex. *J. Neurosci.* 35, 14307–14315.
- Götz, M., and Huttner, W.B. (2005). The cell biology of neurogenesis. *Nat. Rev. Mol. Cell Biol.* 6, 777–788.
- Guerrini, R., and Dobyns, W.B. (2014). Malformations of cortical development: clinical features and genetic causes. *Lancet Neurol.* 13, 710–726.
- Hamel, R., Dejarnac, O., Wichit, S., Ekcharyawat, P., Neyret, A., Lupertlop, N., Perera-Lecoin, M., Surasombatpattana, P., Talagnani, L., Thomas, F., et al. (2015). Biology of Zika Virus Infection in Human Skin Cells. *J. Virol.* 89, 8880–8896.
- Hansen, P.E., Ballesteros, M.C., Soila, K., Garcia, L., and Howard, J.M. (1993). MR imaging of the developing human brain. Part 1. Prenatal development. *Radiographics* 13, 21–36.
- Hansen, D.V., Lui, J.H., Parker, P.R., and Kriegstein, A.R. (2010). Neurogenic radial glia in the outer subventricular zone of human neocortex. *Nature* 464, 554–561.
- Hattori, M., Adachi, H., Tsujimoto, M., Arai, H., and Inoue, K. (1994). Miller-Dieker lissencephaly gene encodes a subunit of brain platelet-activating factor acetylhydrolase [corrected]. *Nature* 370, 216–218.
- Hevner, R.F., and Haydar, T.F. (2012). The (not necessarily) convoluted role of basal radial glia in cortical neurogenesis. *Cereb. Cortex* 22, 465–468.
- Hevner, R.F., Hodge, R.D., Daza, R.A., and Englund, C. (2006). Transcription factors in glutamatergic neurogenesis: conserved programs in neocortex, cerebellum, and adult hippocampus. *Neurosci. Res.* 55, 223–233.
- Heymann, D.L., Hodgson, A., Sall, A.A., Freedman, D.O., Staples, J.E., Althabe, F., Baruah, K., Mahmud, G., Kandun, N., Vasconcelos, P.F.C., et al.

- (2016). Zika virus and microcephaly: why is this situation a PHEIC? *Lancet* **387**, 719–721.
- Hirotsune, S., Fleck, M.W., Gambello, M.J., Bix, G.J., Chen, A., Clark, G.D., Ledbetter, D.H., McBain, C.J., and Wynshaw-Boris, A. (1998). Graded reduction of Pafah1b1 (Lis1) activity results in neuronal migration defects and early embryonic lethality. *Nat. Genet.* **19**, 333–339.
- Hu, W.F., Chahrour, M.H., and Walsh, C.A. (2014). The diverse genetic landscape of neurodevelopmental disorders. *Annu. Rev. Genomics Hum. Genet.* **15**, 195–213.
- Kadoshima, T., Sakaguchi, H., Nakano, T., Soen, M., Ando, S., Eiraku, M., and Sasai, Y. (2013). Self-organization of axial polarity, inside-out layer pattern, and species-specific progenitor dynamics in human ES cell-derived neocortex. *Proc. Natl. Acad. Sci. USA* **110**, 20284–20289.
- Kato, M., and Dobyns, W.B. (2003). Lissencephaly and the molecular basis of neuronal migration. *Hum. Mol. Genet.* **12**, R89–R96.
- Kreitzer, F.R., Salomonis, N., Sheehan, A., Huang, M., Park, J.S., Spindler, M.J., Lizarraga, P., Weiss, W.A., So, P.L., and Conklin, B.R. (2013). A robust method to derive functional neural crest cells from human pluripotent stem cells. *Am. J. Stem Cells* **2**, 119–131.
- LaMonica, B.E., Lui, J.H., Hansen, D.V., and Kriegstein, A.R. (2013). Mitotic spindle orientation predicts outer radial glial cell generation in human neocortex. *Nat. Commun.* **4**, 1665.
- Landriani, M., Capretti, M.G., Lazzarotto, T., Gabrielli, L., Rizzollo, S., Mostert, M., and Manzoni, P. (2012). Neuroimaging in CMV congenital infected neonates: how and when. *Early Hum. Dev.* **88** (Suppl 2), S3–S5.
- Lancaster, M.A., Renner, M., Martin, C.-A., Wenzel, D., Bicknell, L.S., Hurles, M.E., Horwitz, T., Penninger, J.M., Jackson, A.P., and Knoblich, J.A. (2013). Cerebral organoids model human brain development and microcephaly. *Nature* **501**, 373–379.
- Ledbetter, S.A., Kuwano, A., Dobyns, W.B., and Ledbetter, D.H. (1992). Microdeletions of chromosome 17p13 as a cause of isolated lissencephaly. *Am. J. Hum. Genet.* **50**, 182–189.
- Leone, D.P., Srinivasan, K., Chen, B., Alcamo, E., and McConnell, S.K. (2008). The determination of projection neuron identity in the developing cerebral cortex. *Curr. Opin. Neurobiol.* **18**, 28–35.
- Lo Nigro, C., Chong, C.S., Smith, A.C., Dobyns, W.B., Carrozzo, R., and Ledbetter, D.H. (1997). Point mutations and an intragenic deletion in LIS1, the lissencephaly causative gene in isolated lissencephaly sequence and Miller-Dieker syndrome. *Hum. Mol. Genet.* **6**, 157–164.
- Lui, J.H., Hansen, D.V., and Kriegstein, A.R. (2011). Development and evolution of the human neocortex. *Cell* **146**, 18–36.
- Lukaszewicz, A., Savatier, P., Cortay, V., Giroud, P., Huissoud, C., Berland, M., Kennedy, H., and Dehay, C. (2005). G1 phase regulation, area-specific cell cycle control, and cytoarchitectonics in the primate cortex. *Neuron* **47**, 353–364.
- Martin, E., Kikinis, R., Zuerrer, M., Boesch, C., Briner, J., Kewitz, G., and Kaelin, P. (1988). Developmental stages of human brain: an MR study. *J. Comput. Assist. Tomogr.* **12**, 917–922.
- Mlakar, J., Korva, M., Tul, N., Popović, M., Poljsak-Prijatelj, M., Mraz, J., Kolenc, M., Resman Rus, K., Vesnaver Vipontik, T., Fabjan Vodusek, V., et al. (2016). Zika Virus Associated with Microcephaly. *N. Engl. J. Med.* **374**, 951–958.
- Molyneaux, B.J., Arlotta, P., Hirata, T., Hibi, M., and Macklis, J.D. (2005). Fezl is required for the birth and specification of corticospinal motor neurons. *Neuron* **47**, 817–831.
- Moon, H.M., Youn, Y.H., Pemble, H., Yingling, J., Wittmann, T., and Wynshaw-Boris, A. (2014). LIS1 controls mitosis and mitotic spindle organization via the LIS1-NDEL1-dynein complex. *Hum. Mol. Genet.* **23**, 449–466.
- Nagamani, S.C., Zhang, F., Shchelochkov, O.A., Bi, W., Ou, Z., Scaglia, F., Probst, F.J., Shinawi, M., Eng, C., Hunter, J.V., et al. (2009). Microdeletions including YWHAE in the Miller-Dieker syndrome region on chromosome 17p13.3 result in facial dysmorphisms, growth restriction, and cognitive impairment. *J. Med. Genet.* **46**, 825–833.
- Nowakowski, T.J., Pollen, A.A., Sandoval-Espinosa, C., and Kriegstein, A.R. (2016a). Transformation of the Radial Glia Scaffold Demarcates Two Stages of Human Cerebral Cortex Development. *Neuron* **91**, 1219–1227.
- Nowakowski, T.J., Pollen, A.A., Di Lullo, E., Sandoval-Espinosa, C., Bershteyn, M., and Kriegstein, A.R. (2016b). Expression Analysis Highlights AXL as a Candidate Zika Virus Entry Receptor in Neural Stem Cells. *Cell Stem Cell* **18**, 591–596.
- Okita, K., Matsumura, Y., Sato, Y., Okada, A., Morizane, A., Okamoto, S., Hong, H., Nakagawa, M., Tanabe, K., Tezuka, K., et al. (2011). A more efficient method to generate integration-free human iPS cells. *Nat. Methods* **8**, 409–412.
- O'Leary, D.R., Kuhn, S., Kniss, K.L., Hinckley, A.F., Rasmussen, S.A., Pape, W.J., Kightlinger, L.K., Beecham, B.D., Miller, T.K., Neitzel, D.F., et al. (2006). Birth outcomes following West Nile Virus infection of pregnant women in the United States: 2003–2004. *Pediatrics* **117**, e537–e545.
- Oliveira Melo, A.S., Malinger, G., Ximenes, R., Szejnfeld, P.O., Alves Sampaio, S., and Bispo de Filippis, A.M. (2016). Zika virus intrauterine infection causes fetal brain abnormality and microcephaly: tip of the iceberg? *Ultrasound Obstet. Gynecol.* **47**, 6–7.
- Ostrem, B.E., Lui, J.H., Gertz, C.C., and Kriegstein, A.R. (2014). Control of outer radial glial stem cell mitosis in the human brain. *Cell Rep.* **8**, 656–664.
- Park, I.H., Zhao, R., West, J.A., Yabuuchi, A., Huo, H., Ince, T.A., Lerou, P.H., Lensch, M.W., and Daley, G.Q. (2008). Reprogramming of human somatic cells to pluripotency with defined factors. *Nature* **451**, 141–146.
- Pawlisz, A.S., Mutch, C., Wynshaw-Boris, A., Chenn, A., Walsh, C.A., and Feng, Y. (2008). Lis1-Nde1-dependent neuronal fate control determines cerebral cortical size and lamination. *Hum. Mol. Genet.* **17**, 2441–2455.
- Pilaz, L.J., McMahon, J.J., Miller, E.E., Lennox, A.L., Suzuki, A., Salmon, E., and Silver, D.L. (2016). Prolonged Mitosis of Neural Progenitors Alters Cell Fate in the Developing Brain. *Neuron* **89**, 83–99.
- Pilz, D.T., Macha, M.E., Precht, K.S., Smith, A.C., Dobyns, W.B., and Ledbetter, D.H. (1998). Fluorescence in situ hybridization analysis with LIS1 specific probes reveals a high deletion mutation rate in isolated lissencephaly sequence. *Genet. Med.* **1**, 29–33.
- Pollen, A.A., Nowakowski, T.J., Chen, J., Retallack, H., Sandoval-Espinosa, C., Nicholas, C.R., Shuga, J., Liu, S.J., Oldham, M.C., Diaz, A., et al. (2015). Molecular identity of human outer radial glia during cortical development. *Cell* **163**, 55–67.
- Pramparo, T., Youn, Y.H., Yingling, J., Hirotsume, S., and Wynshaw-Boris, A. (2010). Novel embryonic neuronal migration and proliferation defects in Dcx mutant mice are exacerbated by Lis1 reduction. *J. Neurosci.* **30**, 3002–3012.
- Qian, X., Nguyen, H.N., Song, M.M., Hadiono, C., Ogden, S.C., Hammack, C., Yao, B., Hamersky, G.R., Jacob, F., Zhong, C., et al. (2016). Brain-Region-Specific Organoids Using Mini-bioreactors for Modeling ZIKV Exposure. *Cell* **165**, 1238–1254.
- Reillo, I., de Juan Romero, C., García-Cabezas, M.Á., and Borrell, V. (2011). A role for intermediate radial glia in the tangential expansion of the mammalian cerebral cortex. *Cereb. Cortex* **21**, 1674–1694.
- Reiner, O., Carrozzo, R., Shen, Y., Wehnert, M., Faustinella, F., Dobyns, W.B., Caskey, C.T., and Ledbetter, D.H. (1993). Isolation of a Miller-Dieker lissencephaly gene containing G protein beta-subunit-like repeats. *Nature* **364**, 717–721.
- Saito, T., Hanai, S., Takashima, S., Nakagawa, E., Okazaki, S., Inoue, T., Miyata, R., Hoshino, K., Akashi, T., Sasaki, M., et al. (2011). Neocortical layer formation of human developing brains and lissencephalies: consideration of layer-specific marker expression. *Cereb. Cortex* **21**, 588–596.
- Schuler-Faccini, L., Ribeiro, E.M., Feitosa, I.M., Horovitz, D.D., Cavalcanti, D.P., Pessoa, A., Dorigui, M.J., Neri, J.I., Neto, J.M., Wanderley, H.Y., et al.; Brazilian Medical Genetics Society-Zika Embryopathy Task Force (2016). Possible Association Between Zika Virus Infection and Microcephaly - Brazil, 2015. *MMWR Morb. Mortal. Wkly. Rep.* **65**, 59–62.
- Sheen, V.L., Ferland, R.J., Harney, M., Hill, R.S., Neal, J., Banham, A.H., Brown, P., Chenn, A., Corbo, J., Hecht, J., et al. (2006a). Impaired proliferation

- and migration in human Miller-Dieker neural precursors. *Ann. Neurol.* 60, 137–144.
- Sheen, V.L., Ferland, R.J., Neal, J., Harney, M., Hill, R.S., Banham, A., Brown, P., Chenn, A., Corbo, J., Hecht, J., et al. (2006b). Neocortical neuronal arrangement in Miller-Dieker syndrome. *Acta Neuropathol.* 111, 489–496.
- Shi, Y., Kirwan, P., Smith, J., Robinson, H.P.C., and Livesey, F.J. (2012). Human cerebral cortex development from pluripotent stem cells to functional excitatory synapses. *Nat. Neurosci.* 15, 477–486, S1.
- Shitamukai, A., Konno, D., and Matsuzaki, F. (2011). Oblique radial glial divisions in the developing mouse neocortex induce self-renewing progenitors outside the germinal zone that resemble primate outer subventricular zone progenitors. *J. Neurosci.* 31, 3683–3695.
- Shu, T., Ayala, R., Nguyen, M.D., Xie, Z., Gleeson, J.G., and Tsai, L.H. (2004). Ndel1 operates in a common pathway with LIS1 and cytoplasmic dynein to regulate cortical neuronal positioning. *Neuron* 44, 263–277.
- Sidman, R.L., and Rakic, P. (1973). Neuronal migration, with special reference to developing human brain: a review. *Brain Res.* 62, 1–35.
- Silver, D.L., Watkins-Chow, D.E., Schreck, K.C., Pierfelice, T.J., Larson, D.M., Burnett, A.J., Liaw, H.J., Myung, K., Walsh, C.A., Gaiano, N., and Pavan, W.J. (2010). The exon junction complex component Magoh controls brain size by regulating neural stem cell division. *Nat. Neurosci.* 13, 551–558.
- Smart, I.H., Dehay, C., Giroud, P., Berland, M., and Kennedy, H. (2002). Unique morphological features of the proliferative zones and postmitotic compartments of the neural epithelium giving rise to striate and extrastriate cortex in the monkey. *Cereb. Cortex* 12, 37–53.
- Smith, D.S., Niethammer, M., Ayala, R., Zhou, Y., Gambello, M.J., Wynshaw-Boris, A., and Tsai, L.H. (2000). Regulation of cytoplasmic dynein behaviour and microtubule organization by mammalian Lis1. *Nat. Cell Biol.* 2, 767–775.
- Stahl, R., Walcher, T., De Juan Romero, C., Pilz, G.A., Cappello, S., Irmler, M., Sanz-Aquela, J.M., Beckers, J., Blum, R., Borrell, V., and Götz, M. (2013). Trnp1 regulates expansion and folding of the mammalian cerebral cortex by control of radial glial fate. *Cell* 153, 535–549.
- Stiles, J., and Jernigan, T.L. (2010). The basics of brain development. *Neuropsychol. Rev.* 20, 327–348.
- Takahashi, K., Tanabe, K., Ohnuki, M., Narita, M., Ichisaka, T., Tomoda, K., and Yamanaka, S. (2007). Induction of pluripotent stem cells from adult human fibroblasts by defined factors. *Cell* 131, 861–872.
- Tanaka, T., Serneo, F.F., Higgins, C., Gambello, M.J., Wynshaw-Boris, A., and Gleeson, J.G. (2004). Lis1 and doublecortin function with dynein to mediate coupling of the nucleus to the centrosome in neuronal migration. *J. Cell Biol.* 165, 709–721.
- Tang, H., Hammack, C., Ogden, S.C., Wen, Z., Qian, X., Li, Y., Yao, B., Shin, J., Zhang, F., Lee, E.M., et al. (2016). Zika Virus Infects Human Cortical Neural Progenitors and Attenuates Their Growth. *Cell Stem Cell* 18, 587–590.
- Taverna, E., Götz, M., and Huttner, W.B. (2014). The cell biology of neurogenesis: toward an understanding of the development and evolution of the neocortex. *Annu. Rev. Cell Dev. Biol.* 30, 465–502.
- Teissier, N., Fallet-Bianco, C., Delezoide, A.L., Laquerrière, A., Marcorelles, P., Khung-Savatovsky, S., Nardelli, J., Cipriani, S., Csaba, Z., Picone, O., et al. (2014). Cytomegalovirus-induced brain malformations in fetuses. *J. Neuropathol. Exp. Neurol.* 73, 143–158.
- Toyo-oka, K., Shionoya, A., Gambello, M.J., Cardoso, C., Leventer, R., Ward, H.L., Ayala, R., Tsai, L.H., Dobyns, W., Ledbetter, D., et al. (2003). 14-3-3epsilon is important for neuronal migration by binding to NUDEL: a molecular explanation for Miller-Dieker syndrome. *Nat. Genet.* 34, 274–285.
- Wang, X., Tsai, J.W., LaMonica, B., and Kriegstein, A.R. (2011). A new subtype of progenitor cell in the mouse embryonic neocortex. *Nat. Neurosci.* 14, 555–561.
- Xie, Y., Jüschke, C., Esk, C., Hirotsume, S., and Knoblich, J.A. (2013). The phosphatase PP4c controls spindle orientation to maintain proliferative symmetric divisions in the developing neocortex. *Neuron* 79, 254–265.
- Yingling, J., Youn, Y.H., Darling, D., Toyo-Oka, K., Pramparo, T., Hirotsume, S., and Wynshaw-Boris, A. (2008). Neuroepithelial stem cell proliferation requires LIS1 for precise spindle orientation and symmetric division. *Cell* 132, 474–486.
- Youn, Y.H., Pramparo, T., Hirotsume, S., and Wynshaw-Boris, A. (2009). Distinct dose-dependent cortical neuronal migration and neurite extension defects in Lis1 and Ndel1 mutant mice. *J. Neurosci.* 29, 15520–15530.
- Yu, J., Vodyanik, M.A., Smuga-Otto, K., Antosiewicz-Bourget, J., Frane, J.L., Tian, S., Nie, J., Jonsdottir, G.A., Ruotti, V., Stewart, R., et al. (2007). Induced pluripotent stem cell lines derived from human somatic cells. *Science* 318, 1917–1920.

STAR★METHODS**KEY RESOURCES TABLE**

REAGENT or RESOURCE	SOURCE	IDENTIFIER
Antibodies		
PAX6	Covance	PRB-278P
SOX2	Santa Cruz	Sc-17320
p-VIMENTIN	MBL (ser82)	D095-3
p-VIMENTIN	Abcam (ser55)	Ab22651
SOX1	R&D Systems	AF3369
N-CADHERIN	BD Bioscience	610920
Cleaved CASPASE 3	Cell Signaling Technology	9661S
Ki67	BD PharMingen	550609
PKC ζ	Santa Cruz	Sc-216
PERICENTRIN	Abcam	Ab4448
p-HISTONE H3	Abcam	Ab10543
TBR2	Millipore	AB15894
CTIP2	Abcam	Ab18465
DCX	Millipore	AB2253
β III TUBULIN	Covance	MMS-435P
PARD6b	Santa Cruz	Sc-166405
GFP	Aves Labs	GFP-1020
PTPRZ1	Sigma	HPA015103
TNC	Abcam	Ab108930
SATB2	Abcam	Ab51502
BLBP	Millipore	ABN14
Chemicals, Peptides, and Recombinant Proteins		
FBS	HyClone	Cat# SH30071.03
Accutase	Stem Cell Technologies	Cat# 07920
ReleSR	Stem Cell Technologies	Cat# 05872
Growth Factor-Reduced Matrigel	BD Biosciences	Cat# 354263
Y-27632	Tocris	Cat# 1254
IWR1- ϵ	Cayman Chemical	Cat# 13659
SB431542	Tocris	Cat# 1614
Glutamax	Lifetech	Cat# 10565-018
N2 supplement	Lifetech	Cat# 17502-048
Lipid Concentrate	Lifetech	Cat# 11905-031
Heparin	Sigma	Cat# H3149
Critical Commercial Assays		
RNeasy mini kit	QIAGEN	Cat# 74104
RNase-Free DNase Set	QIAGEN	Cat# 79254
iScript cDNA synthesis kit	Biorad	Cat# 1708891
SsoFast EvaGreen Supermix	Biorad	Cat# 1725201
SMARTer Ultra Low RNA Kit	Clontech	Cat# 634833
Nextera XT DNA Sample Preparation Kit	Illumina	Cat# FC-131-1096
Deposited Data		
Single cell RNA sequencing data	This paper	dbGaP: phs000989.v3.p1

(Continued on next page)

Continued

REAGENT or RESOURCE	SOURCE	IDENTIFIER
Experimental Models: Cell Lines		
Human WT iPSC line “BJ-4” derived from healthy newborn male fibroblasts	ATCC (fibroblasts); Conklin lab, UCSF (iPSC line)	BJ-4
Human WT iPSC lines “1323-2” and “1323-4” derived from healthy 48-year-old Caucasian female fibroblasts	Cell Applications; 106-05a (fibroblasts); Conklin lab, UCSF (iPSC lines)	1323-2/1323-4
Human WT iPSC line “WTc” derived from healthy 30-year-old Japanese male fibroblasts	Conklin lab, UCSF (fibroblasts and iPSC line)	WTc-10
Human MDS iPSC line “MDS Rescue” derived from 4-month old Caucasian male with a ring chromosome 17	Coriell Institute for Medical Research (GM06047-fibroblasts); Bershteyn et al. (2014) (iPSC lines)	MDS1r(17)-1
Human MDS iPSC lines “MDS2-9” and “MDS2-10” from 1 year old Caucasian female	Coriell Institute for Medical Research (GM06097-fibroblasts); Bershteyn et al. (2014) (iPSC lines)	MDS2-9/MDS2-10
Human MDS iPSC lines “MDS3-3” and “MDS3-4” from 18 fetal weeks male	Coriell Institute for Medical Research (GM09208-fibroblasts); Bershteyn et al. (2014) (iPSC lines)	MDS3-3/MDS3-4
Human MDS iPSC lines “MDS4-4” and “MDS4-15” from six month old Caucasian female	This paper	MDS4-4/MDS4-15
Recombinant DNA		
Ad-CMV-eGFP	Vector Biolabs	Cat# 1060
AAV1-CAG-tdTomato	University of Pennsylvania Vectorcore	N/A
Software and Algorithms		
Imaris	Bitplane	http://www.bitplane.com/Default.aspx?tabid=423#imaris
Singular Analysis Toolset	Fluidigm	https://www.fluidigm.com/software
GENE-E	Broad Institute	https://software.broadinstitute.org/GENE-E/download.html

CONTACT FOR REAGENT AND RESOURCE SHARING

Further information and requests for reagents may be directed to, and will be fulfilled by the lead contact, Dr. Arnold Kriegstein (KriegsteinA@stemcell.ucsf.edu).

EXPERIMENTAL MODEL AND SUBJECT DETAILS**hiPSC derivation and culture methods**

All human iPSC studies were approved by the UCSF Committee on Human Research and the UCSF GESCR (Gamete, Embryo, and Stem Cell Research) Committee. All the iPSC lines were generated and characterized previously ([Kreitzer et al., 2013](#); [Bershteyn et al., 2014](#)). Briefly, three micrograms of episomal expression plasmid mixture encoding OCT3/4, SOX2, KLF4, L-MYC, LIN28, and shRNA for TP53 (Y4 mixture, [Okita et al., 2011](#)) were electroporated into 3×10^5 fibroblasts with a Neon Electroporation Device (Invitrogen) with a 100 μ L kit, according to the manufacturer’s instructions. Conditions for electroporations were 1,650V, 10ms, and three pulses. Cells were detached within 1 week after electroporation and seeded at $1-3 \times 10^5$ cells per 10-cm dish onto irradiated or mitomycin-C treated SNL feeder cells. The culture medium was replaced the next day with primate ESC medium (Reprocell) containing β FGF. Colonies were counted 25 days after electroporation, and those colonies similar to hESCs were selected for further cultivation and evaluation. Established hiPSC lines were cultured in mTeSR1 medium (Stem Cell Technologies, 05850) supplemented with Penicillin/Streptomycin/Gentomycin on Matrigel-coated dishes. Accutase or ReleSR were used for cell passaging. For a complete list of iPSC lines and experiments, please refer to [Table S2](#).

METHOD DETAILS**Cerebral organoid generation and culture**

Cerebral organoids were generated according to previously published methods ([Kadoshima et al., 2013](#)). Briefly, hiPSCs were dissociated to single cells with Accutase and re-aggregated using cortical differentiation medium in lipidure-coated 96-well V-bottom plates at a density of 10,000 cells per aggregate, 100 μ L per well. The cortical differentiation medium (Glasgow-MEM, 20% KSR,

0.1mM NEAA, 1mM sodium pyruvate, 0.1mM β -ME, 100 U/mL penicillin/streptomycin) was supplemented with Rho Kinase Inhibitor (Y-27632, 20 μ M, days 0-3), WNT inhibitor (IWR1- ϵ , 3 μ M, days 0-18) and TGF- β inhibitor (SB431542, 5 μ M, days 0-18). Media changes were performed on days 3, 6 and then every 2-3 days until day 18. On day 18, the aggregates were transferred to ultra low adhesion 6-well plates in DMEM/F12 medium with Glutamax supplemented with N2, Lipid Concentrate, Fungizone (2.5 μ g/mL), and penicillin/streptomycin (100 U/mL) and grown under 40% O₂ 5% CO₂ conditions. From day 35, FBS (10% v/v), Matrigel (1% v/v) and heparin (5 μ g/mL) were added to the medium.

Quantitative PCR (qPCR)

To isolate RNA, cells were lysed with TRIzol reagent. Following chloroform extraction, aqueous phase containing RNA was mixed with 70% ethanol, transferred onto mini spin column, isolated with RNeasy mini kit, and digested with DNase I. RNA quality and concentration were assessed using a Nanodrop. cDNA was prepared with iScript cDNA synthesis kit. qPCR was done with SsoFast EvaGreen Supermix using a Vii7 instrument (Applied Biosystems). Relative mRNA expression levels were determined by $\Delta\Delta Ct$ method relative to B2M housekeeping control. qPCR data is reported as a mean \pm standard deviation from 3 technical replicates for each of the WT and MDS lines. Primers sequences are available upon request.

Organoid slice culture, viral infection and time-lapse imaging

At 5 and 10 weeks of culture (days 35 and 70, \pm 2 days, respectively), organoids were imbedded in blocks of 3.5% low melting point Agarose dissolved in DMEM. Subsequently, 200- μ m vibratome sections were generated and incubated overnight at 37°C, 8% O₂, 5% CO₂ in organoid culture medium containing AV-CMV-GFP adenovirus (diluted 1:1000) for preferential labeling of dividing progenitors or AAV1-CAG-tdTomato adeno associated virus (diluted 1:100) for preferential labeling of migrating neurons. Following infection (1-2 days for AV, 2-3 days for AAV1), organoid slices were immobilized on glass-bottom dishes (MatTek) using concentrated Matrigel and then overlaid with culture medium. Slices were imaged for 2-5 days using 10x or 20x air objectives on an inverted Leica TCS SP5 microscope with an on-stage environment-controlled chamber, streaming 5% O₂, 5% CO₂, balanced N₂. Imaging was done at 15-20 min intervals for analyzing neuronal progenitor divisions or at 30min-1hr intervals for analyzing neuronal migration. Maximum intensity projections of the collected z stacks were analyzed using Imaris software.

Neuronal migration assays

For the in vitro migration assay, intact organoids were resuspended in concentrated Matrigel using the wide orifice 200 μ L tips, and placed on a glass-bottom surface of 6- or 12-well culture plates (MatTek) (3-4 organoids per well in separate Matrigel drops). The Matrigel was allowed to solidify for 30min at 37°C, and culture medium was then carefully overlaid on top of Matrigel drops (day 0). Processes were observed coming out of the organoids 24 hr later (day 1). Time-lapse imaging was initiated on day 2, and post time-lapse immunostaining was performed on day 3. Cell tracking and end-point analyses were done using Imaris software.

For migration on cortical slice explants, intact organoids were incubated on day 0 with the AAV1-CAG-tdTomato virus at 37°C (1:100). Also on day 0, cortical tissue (GW18.5) was embedded in 3.5% low melting point Agarose in DMEM. Cortical vibratome sections (250- μ m thick) were generated, cut into smaller pieces (of ventricular width similar to the diameter of spheres) and incubated at 37°C, 8% O₂, 5% CO₂ in slice culture medium (66% β ME, 25% Hanks, 5% FBS, 1% N-2, Penicillin/Streptomycin, Glutamine (all from Invitrogen) and 0.66% D-(+)-glucose (Sigma) containing AV-CMV-GFP adenovirus (1:1000). On day 1, organoids and cortical slices were washed to remove residual viral particles and placed against each other on glass bottom dishes. Any residual liquid was removed to allow the pieces of tissues to attach to each other (about 3-5min) and subsequently overlaid with concentrated Matrigel. The Matrigel was allowed to solidify for 30min and 37°C, and organoid and slice culture media (50:50 mixture) was then carefully overlaid on top of Matrigel drops. The endpoint analysis was performed on day 4 using Imaris software.

Immunocytochemistry

Organoids were fixed with 4% PFA in PBS for 20min, washed with PBS, dehydrated with 30% sucrose in PBS overnight at 4°C, imbedded in blocks of 30% sucrose/OCT compound (50:50 mixture) and frozen at -80°C. 16-20 μ m cryosections were subjected to heat/citrate-based antigen retrieval for 20 min, permeabilized and blocked with 10% donkey serum in PBS, 0.1% Triton X-100, 0.2% gelatin. Primary antibody incubations were performed at 4°C overnight and secondary incubations were performed at room temperature for 1-3 hr. After primary and secondary antibody incubations, three 20 min washes in PBS were performed. Secondary antibodies were: AlexaFluor 488, 546, 594, or 647 -conjugated donkey anti-goat, -rabbit, -rat or -mouse IgG (Invitrogen, all used at 1:1000 dilution).

Single Cell RNA-Sequencing

For single cell analysis, organoids from five biological replicates: WT (2 individuals), MDS (3 individual) were dissociated to a single cell suspension for 30 to 60 min using the papain dissociation system (Worthington). Single cells were captured using small cell (5 – 10 μ m) C1 Single-Cell Auto Prep Integrated Fluidic Circuit (IFC, Fluidigm). Reverse transcription and cDNA amplification were performed on the IFC using the SMARTer Ultra Low RNA Kit, and single cell libraries were prepared using the Nextera XT DNA Sample Preparation Kit. Sequencing was performed on a HiSeq 2500 Ultra-High-Throughput Sequencing System (Illumina). Reads were aligned using Tophat2, and the expression of RefSeq genes was quantified by the featureCounts routine.

Outlier removal and enrichment for cortical lineage cells

Chambers with multiple cells as visualized by phase and fluorescent microscopy were discarded from further analyses, leaving 1107 libraries. Gene expression values were normalized based on library size as counts per million reads (CPM). Libraries with fewer than 1,000 genes detected above 1 CPM were eliminated as outliers, leaving 643 libraries. These libraries were further filtered by performing the identifyOutliers routine with default setting from the Singular Analysis Toolset (Fluidigm) in R. Of these 469 single cell libraries passing bioinformatic quality control criteria, 358 libraries expressed the telencephalon marker FOXG1 above 1 CPM, and 274 also lacked inhibitory neuron lineage marker DLX6, suggesting cells belonging to the cortical lineage.

Identification of radial glia-like cells and analysis of heterogeneity

Principal component analysis (PCA) was performed using the prcomp function in R and centering the data to identify the major sources of variation across cells, and k-means clustering (optimal k = 6 was determined using ConsensusClusterPlus R package) of PC 1-5 sample scores was performed followed by multiscale bootstrapping using pvClust package (1000 bootstraps) to determine the approximately unbiased p value for every cluster. This analysis, combined with a supervised analysis of cell identity based on the expression of canonical marker genes revealed 90 dorsal telencephalic radial glia-like in vitro cells. We previously identified genes enriched in all radial glia cells (pan-RG), and genes enriched in oRG and vRG cells (Pollen et al., 2015). We visualized the expression of these marker genes over time and across cells using GENE-E (Broad Institute) and R. To examine whether in vitro-derived radial glia-like cells shared patterns of heterogeneity with primary cells, we evaluated the extent to which gene co-expression relationship among radial glia subtype marker genes are preserved in vitro. We computed the mean pairwise correlation coefficient between oRG marker genes across primary and in vitro cells. We then examined the probability that this observed level of co-expression between oRG markers would appear by chance in a background set of oRG, vRG, and pan-RG markers by calculating the mean pairwise correlation of genes randomly sampled from this combined set of radial glia markers across 100,000 permutations. For in vitro cells, we narrowed the list of radial glia marker genes to genes expressed in at least 10% of cells above log₂CPM of 1.

QUANTIFICATION AND STATISTICAL ANALYSIS

Throughout the paper, independent iPSC clones are treated as biological replicates. For statistical analyses, a single average value is used for each clone after collapsing technical replicates arising from multiple observations in sister organoids and from repeat experiments. On information about which specific iPSC lines were used for each of the experiments, please refer to Table S2. All of the statistical details of experiments can be found in the figure legends.

DATA AND SOFTWARE AVAILABILITY

Data Resources

Normalized gene expression values from single cell RNA sequencing profiling are expressed as log₂ counts per million (CPM) reads for all genes across cells analyzed with more than 1000 genes detected above 1 CPM. The accession number for the single cell sequencing data reported in this paper is dbGaP: phs000989.v3.p1.